Reconnection in Magnetically-Dominated Plasmas

Lorenzo Sironi (Columbia)

Exascale Thinking of Particle Energization Problems

Nordita, Stockholm, August 29th 2017

Magnetic reconnection

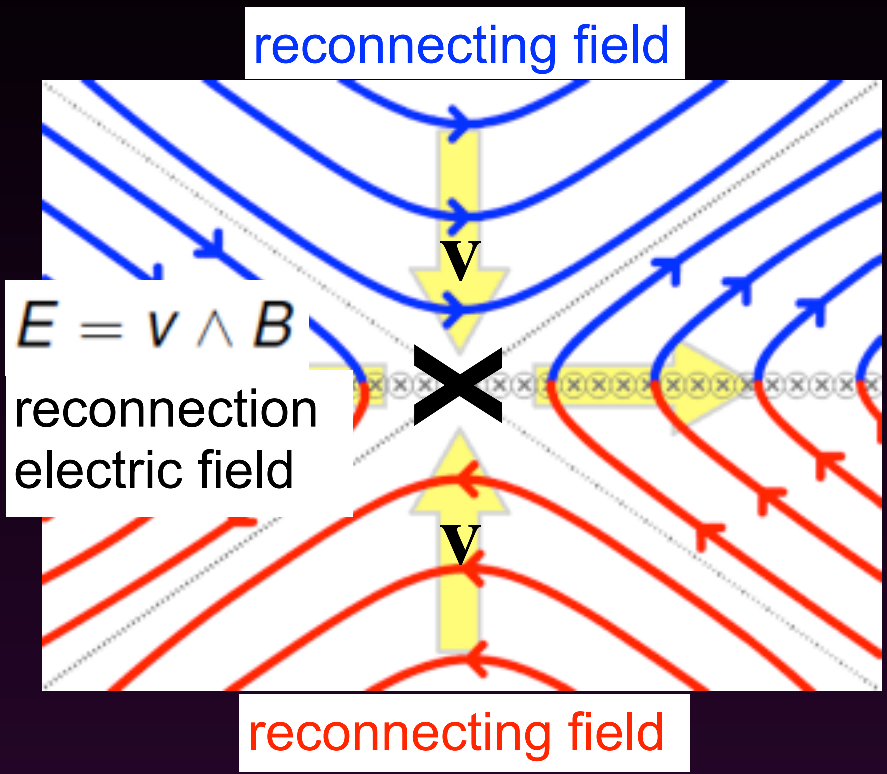

$$\sigma = \frac{B_0^2}{4\pi n_0 m_p c^2}$$

σ≪1

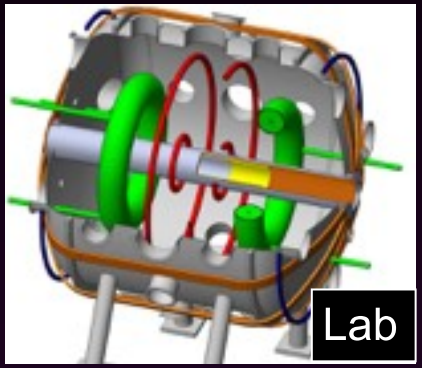

σ≫1

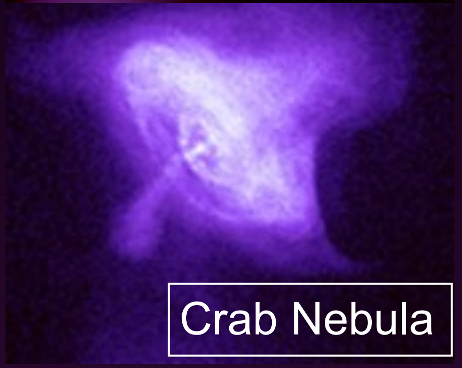

Relativistic Reconnection

$$\sigma = \frac{B_0^2}{4\pi n_0 m_p c^2} \gg 1 \qquad v_A \sim c$$

Relativistic jets are our best “laboratories” of relativistic reconnection

Outline

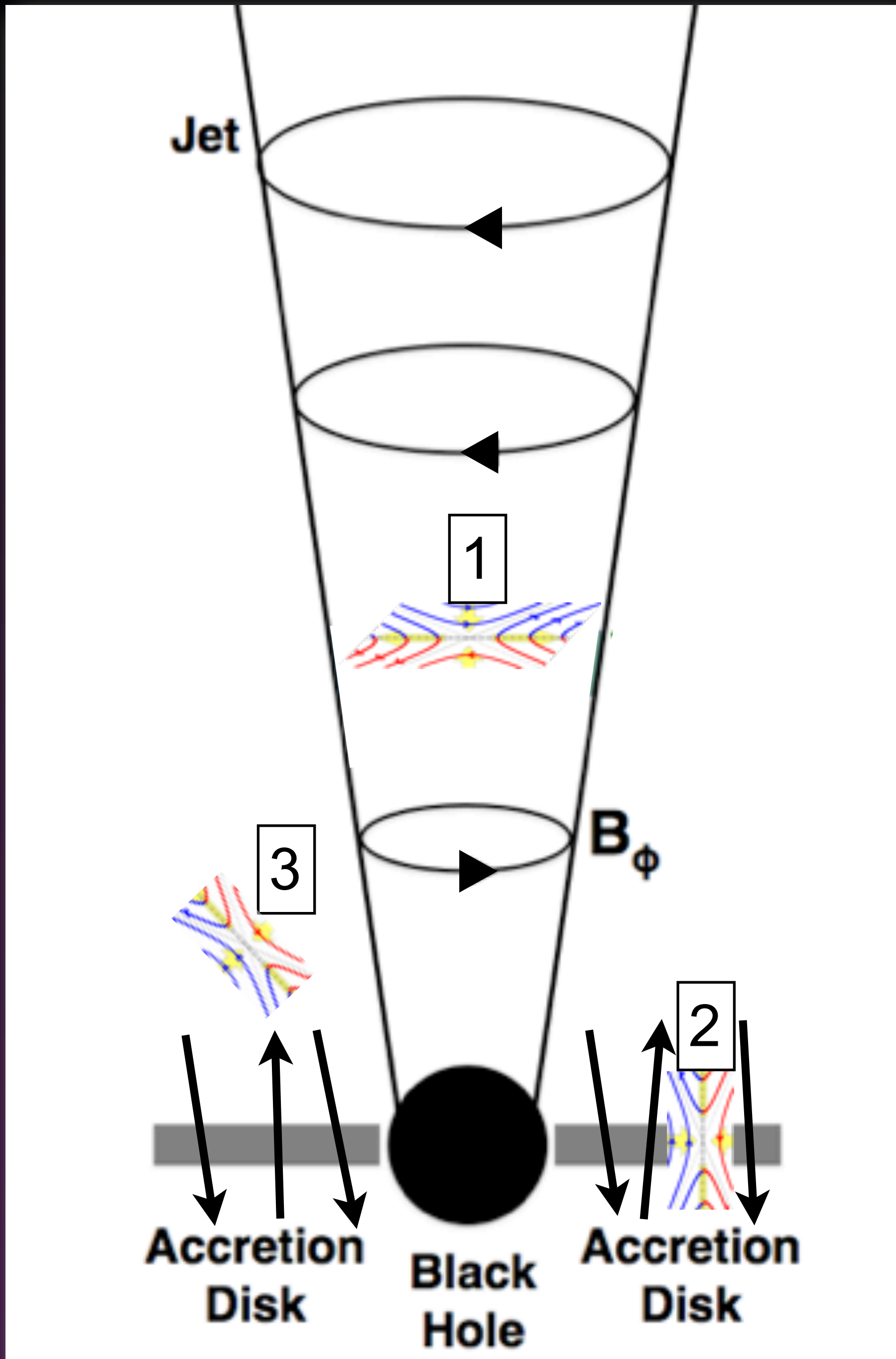

1. Blazar jets (also microquasars, GRB jets, pulsar winds). Ultra-relativistic reconnection ($\sigma \gtrsim$ a few).

2. Collisionless accretion flows (like Sgr A* in our Galactic Center). Trans-relativistic reconnection (σ~1).

3. Magnetized coronae in accreting binaries (Cyg X-1). Reconnection in strong radiation fields.

The PIC method

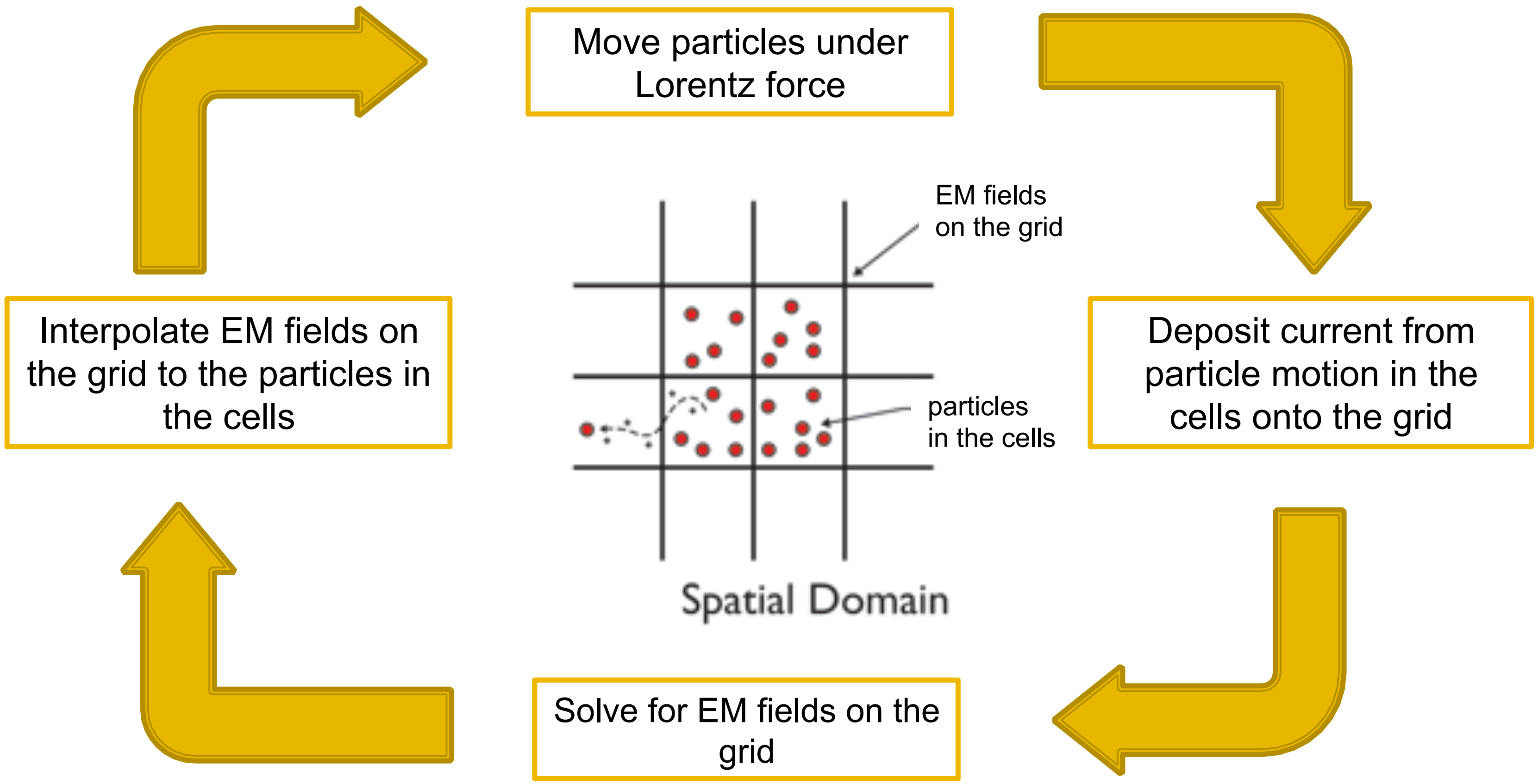

- Relativistic 3D e.m. PIC code TRISTAN-MP (Buneman 93, Spitkovsky 05, LS+ 13)

Simulation setup

Simulation setup

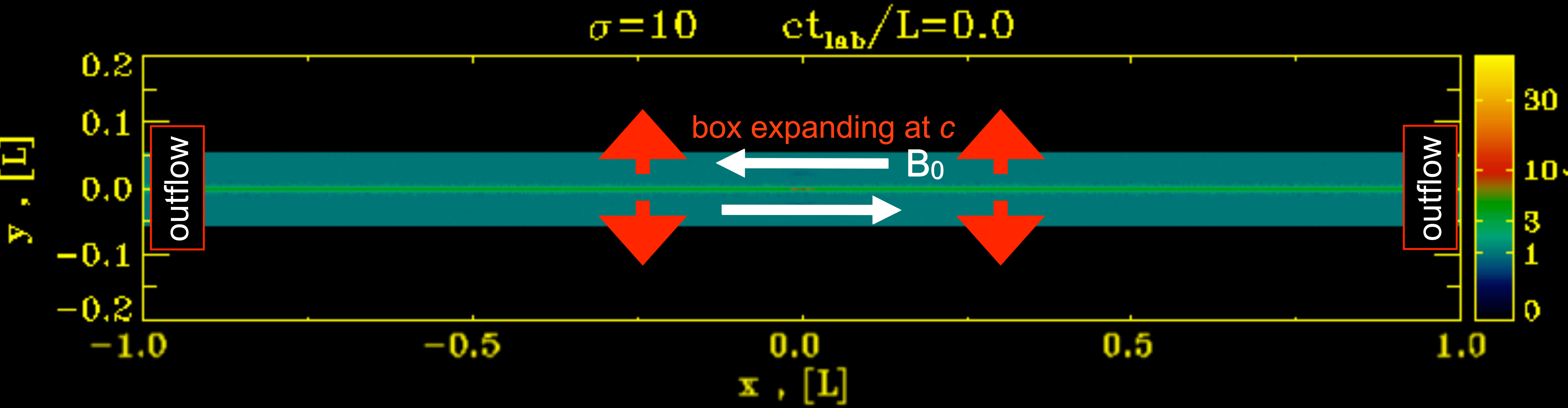

- Inflow direction (y): two receding injectors supply fresh plasma and magnetic flux, the computational box expands over time.
- Outflow direction (x): periodic or outflow boundaries.

- For outflow, particles are deleted, and fields in the absorbing layer satisfy:

$$\frac{\partial \boldsymbol{B}}{\partial t} = -c\nabla \times \boldsymbol{E} - \lambda(x)(\boldsymbol{B} - \boldsymbol{B}_{\rm in})$$
$$\frac{\partial \boldsymbol{E}}{\partial t} = c\nabla \times \boldsymbol{B} - 4\pi \boldsymbol{J} - \lambda(x)\boldsymbol{E}$$

$$\boldsymbol{B}_{\rm in} = -B_0\, \hat{\boldsymbol{x}} \tanh\left(2\pi y/\Delta\right)$$

$$\lambda = (4/\Delta_{\rm abs}\delta t)[|x - x_1|/\Delta_{\rm abs}]^3$$

(LS+ 16, see also Cerutti+ 15, Belyaev 15)

Dynamics and particle spectrum

Inflows and outflows

2D PIC simulation of σ=10 electron-positron reconnection

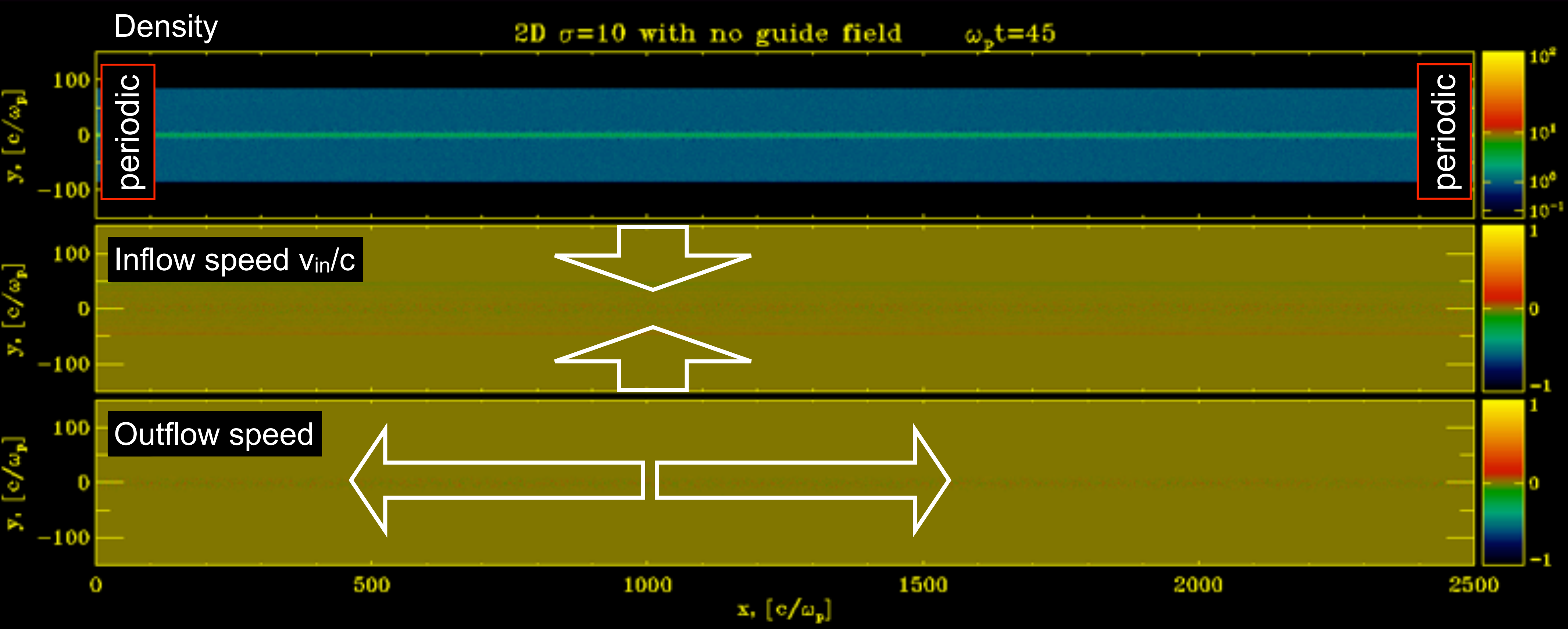

- Inflow into the layer is non-relativistic, at v_{in} ~ 0.1 c (Lyutikov & Uzdensky 03, Lyubarsky 05).
- Outflow from the X-points is ultra-relativistic, reaching the Alfven speed $v_A = c\sqrt{\frac{\sigma}{1+\sigma}}$

3D σ=10 reconnection with no guide field

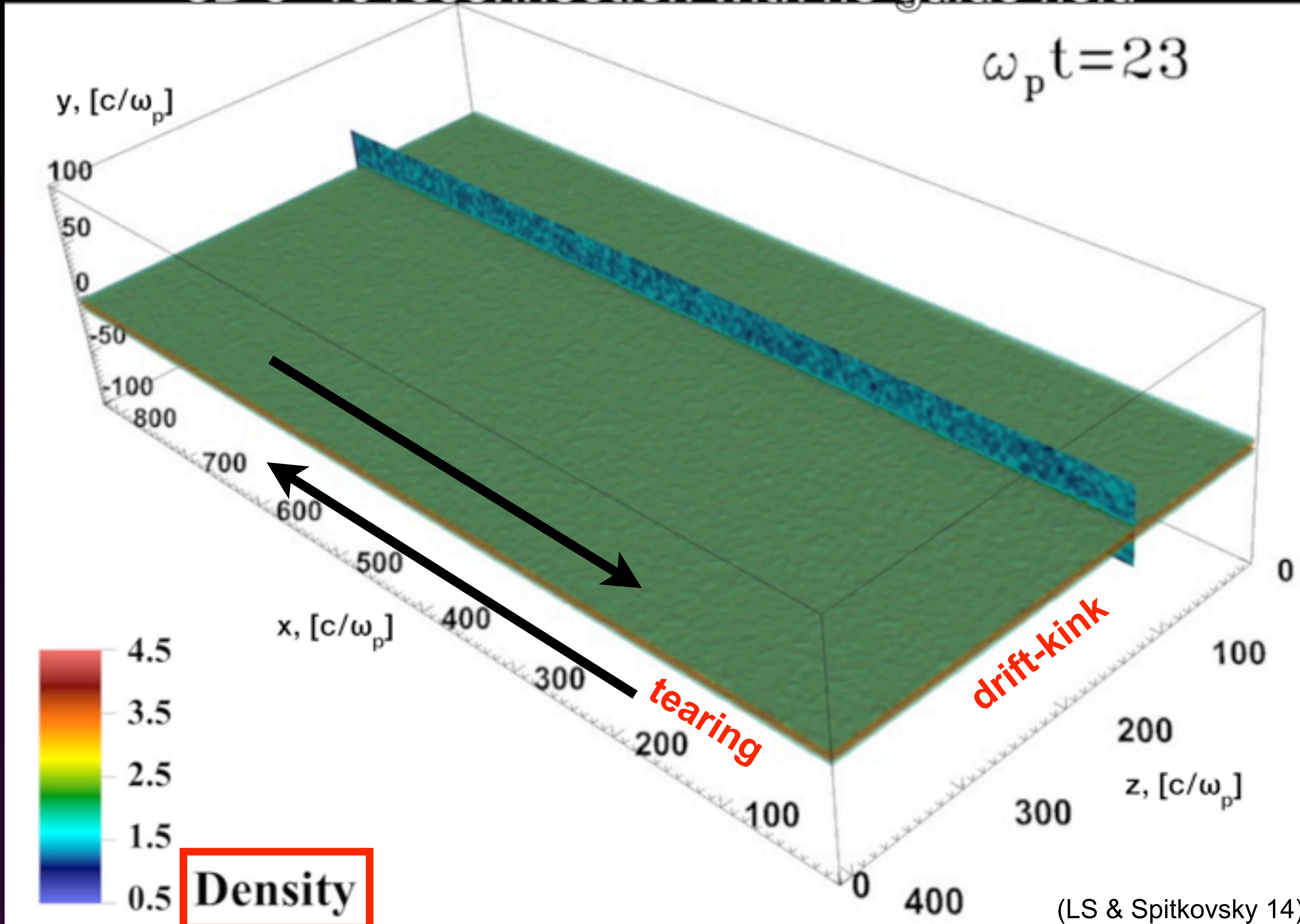

- In 3D, the in-plane tearing mode and the out-of-plane drift-kink mode coexist.
- The drift-kink mode is the fastest to grow, but the physics at late times is governed by the tearing mode, as in 2D.

The particle energy spectrum

- At late times, the particle spectrum approaches a power law $dn/d\gamma \propto \gamma^{-p}$.

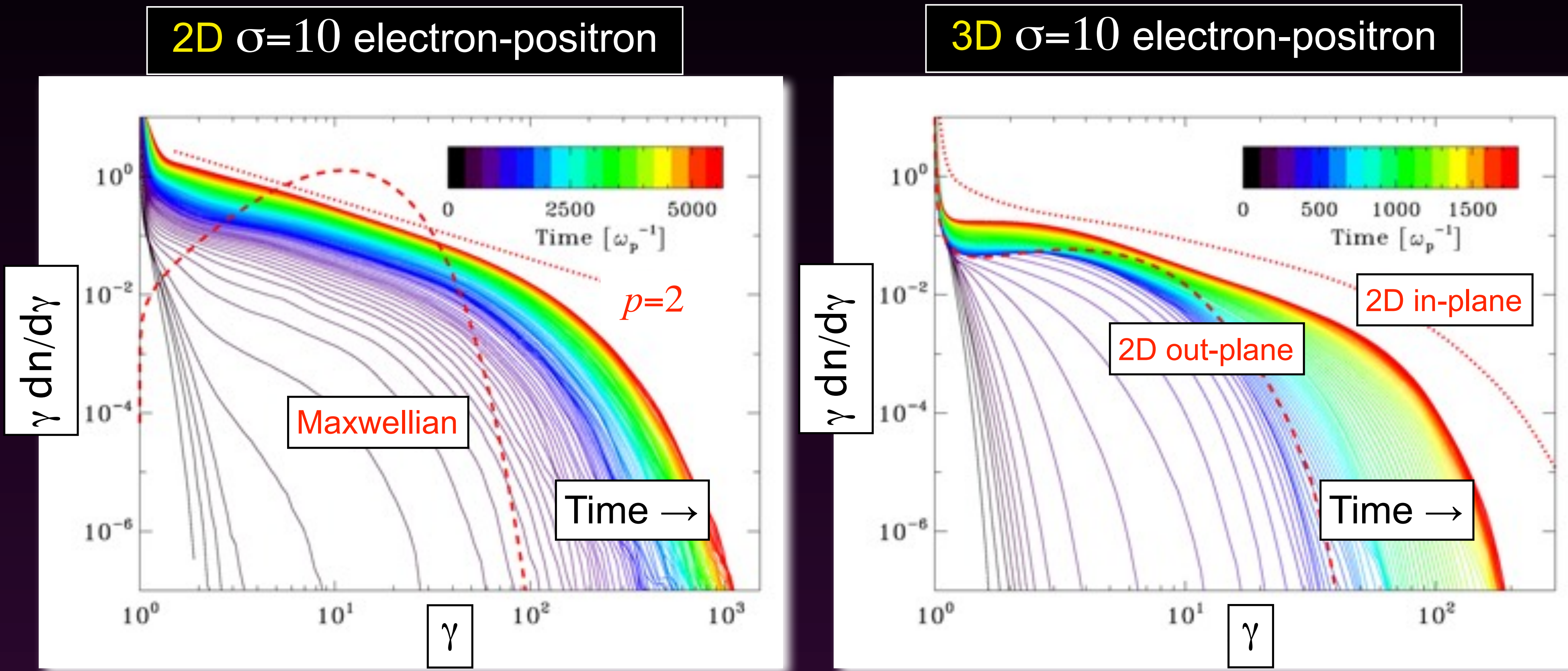

(LS & Spitkovsky 14)

- The max energy grows linearly with time, if the evolution is not artificially inhibited by the boundaries.

1. Reconnection in blazar jets

(A) Extended non-thermal distributions

1ES 0414+009

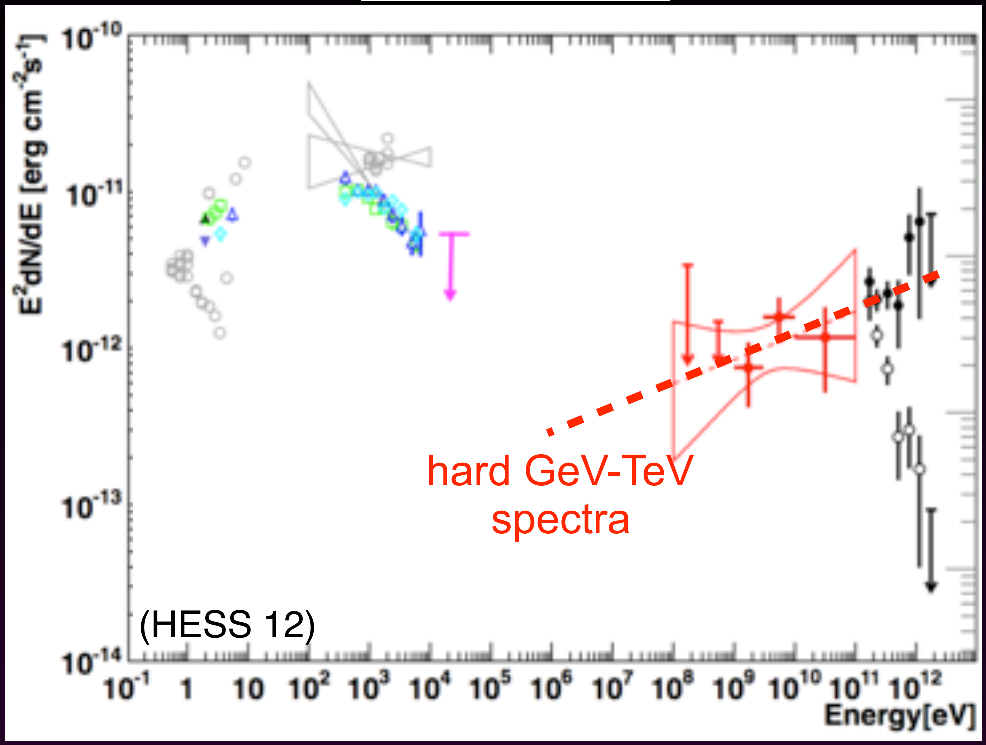

2D electron-positron

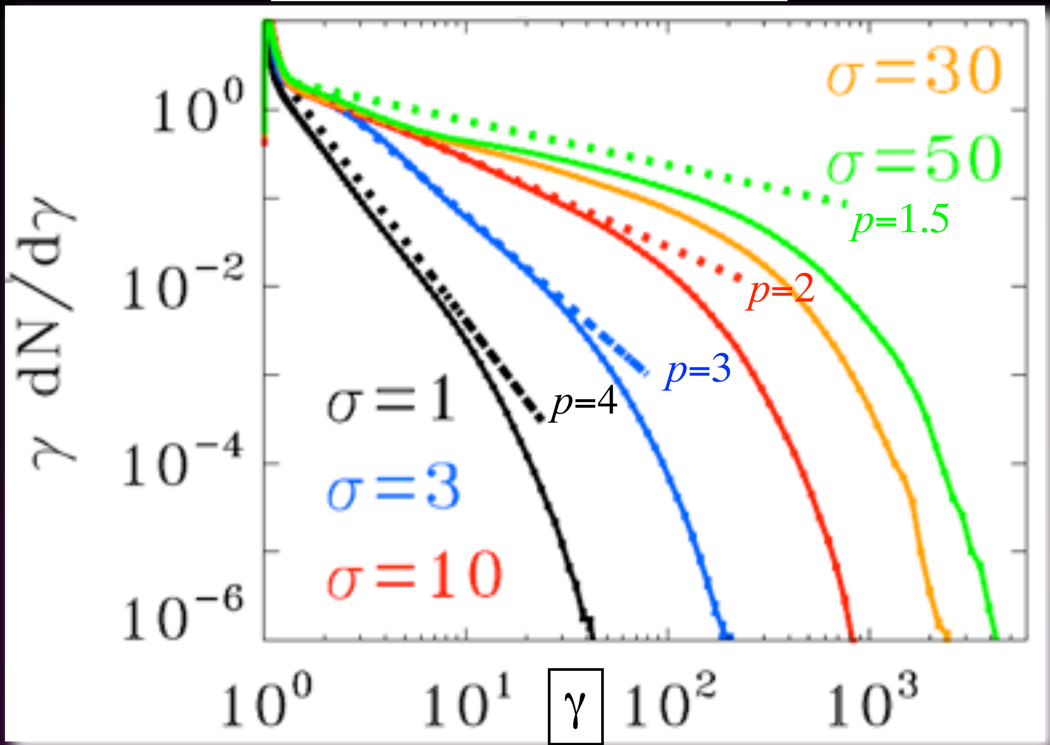

(LS & Spitkovsky 14, see also Melzani+14, Guo+14,15, Werner+16)

Blazar phenomenology:

- extended power-law distributions of the emitting particles, with hard slope

$$\frac{dn}{d\gamma} \propto \gamma^{-p} \qquad p \lesssim 2$$

Relativistic reconnection:

✓ it produces extended non-thermal tails of accelerated particles, whose power-law slope is harder than *p*=2 for high magnetizations (σ>10)

(B) Fast time variability

TeV

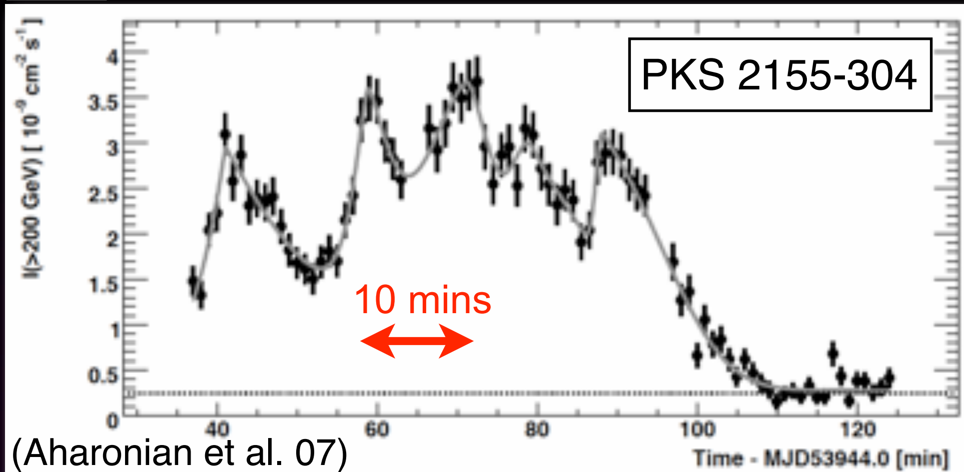

(Aharonian et al. 07)

GeV

3C 279

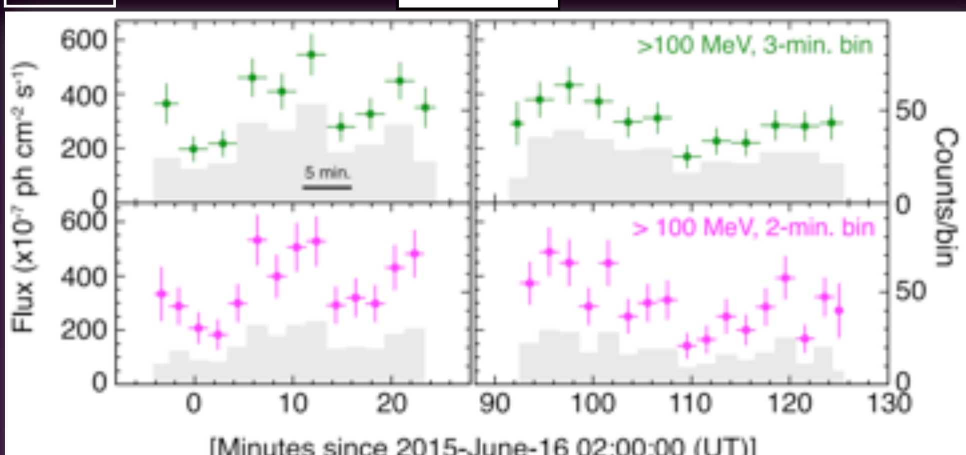

(Ackermann+16)

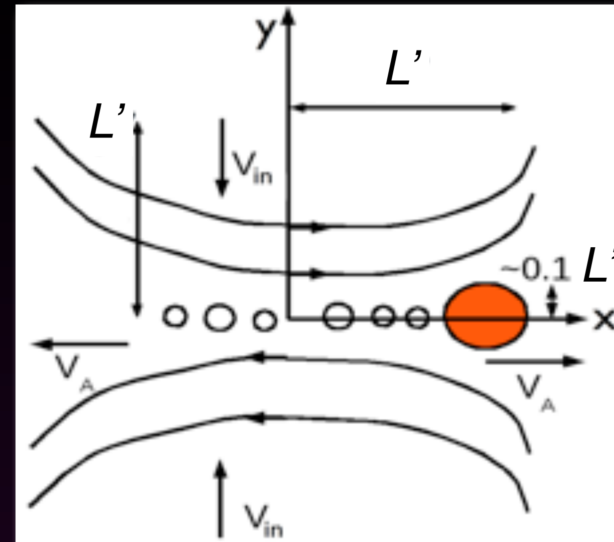

"jets in a jet"

(Giannios 09,13)

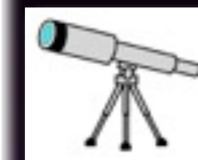

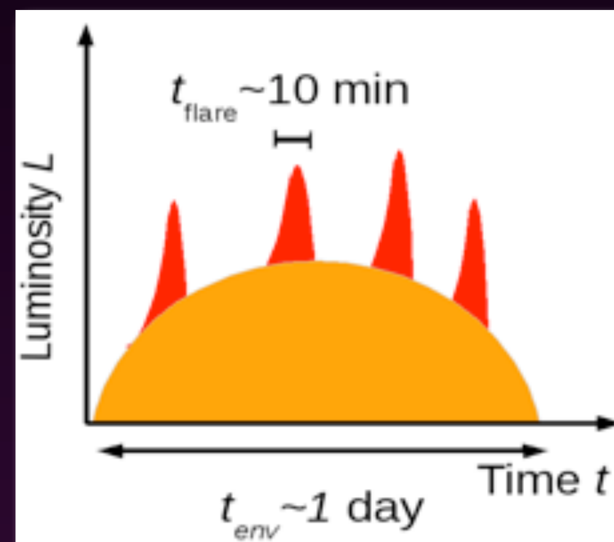

Blazar phenomenology:

- at TeV and GeV energies, fast (~10 minutes) flares

Relativistic reconnection:

✓ the fast islands/plasmoids can be a promising source of short-time variability

Plasmoids in reconnection layers

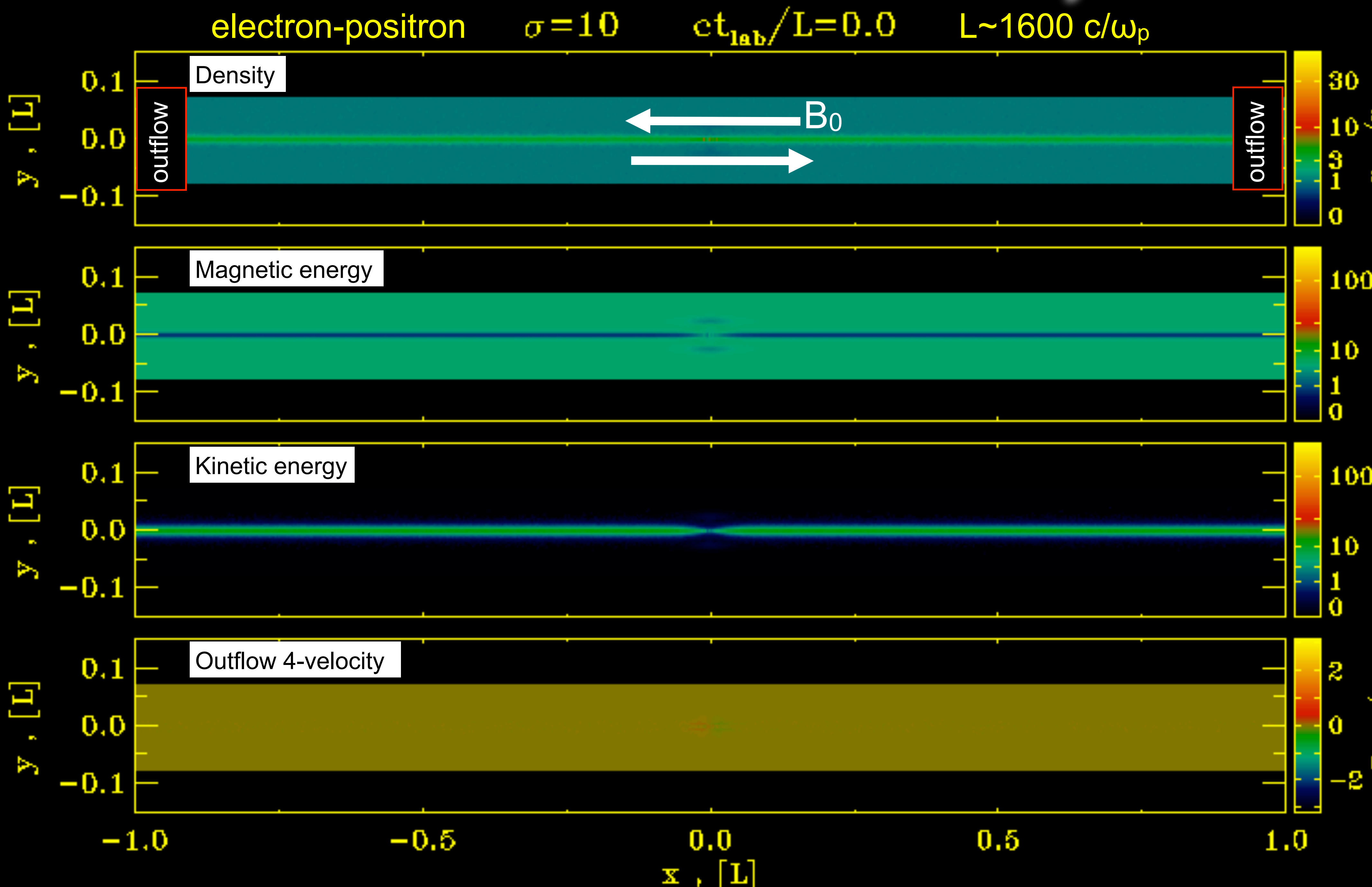

(LS, Giannios & Petropoulou 16)

Plasmoid fluid properties

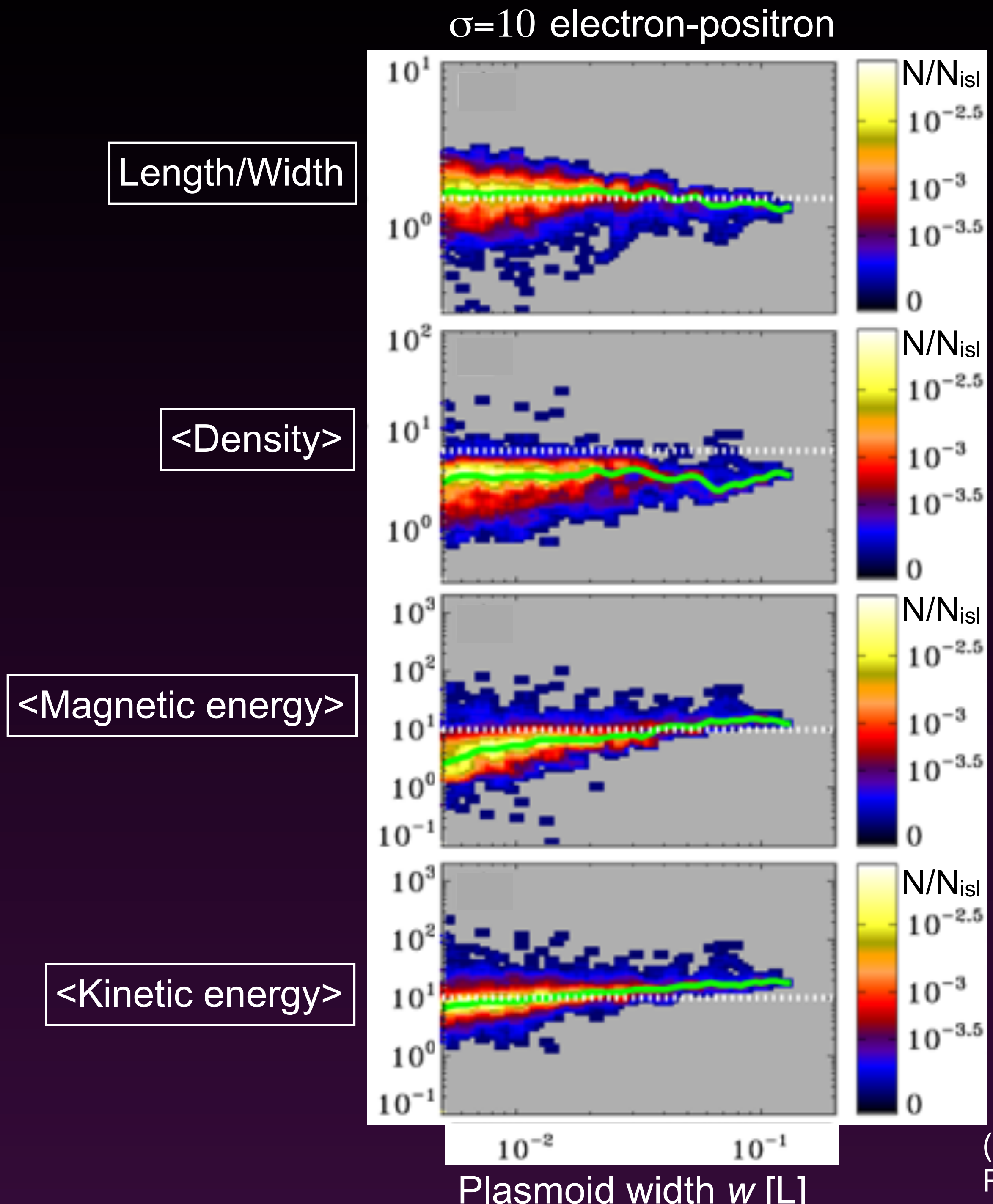

Plasmoids fluid properties:

- they are nearly spherical, with Length/Width~1.5 (regardless of the plasmoid width *w*).

- they are over-dense by ~ a few with respect to the inflow region (regardless of *w*).

- $\varepsilon_B \sim \sigma$, corresponding to a magnetic field compressed by $\sim\sqrt{2}$ (regardless of *w*).

- $\varepsilon_{kin} \sim \varepsilon_B \sim \sigma \rightarrow$ equipartition (regardless of *w*).

(LS, Giannios & Petropoulou 16)

Plasmoid statistics

Cumulative distribution of size　　Cumulative distribution of magnetic flux

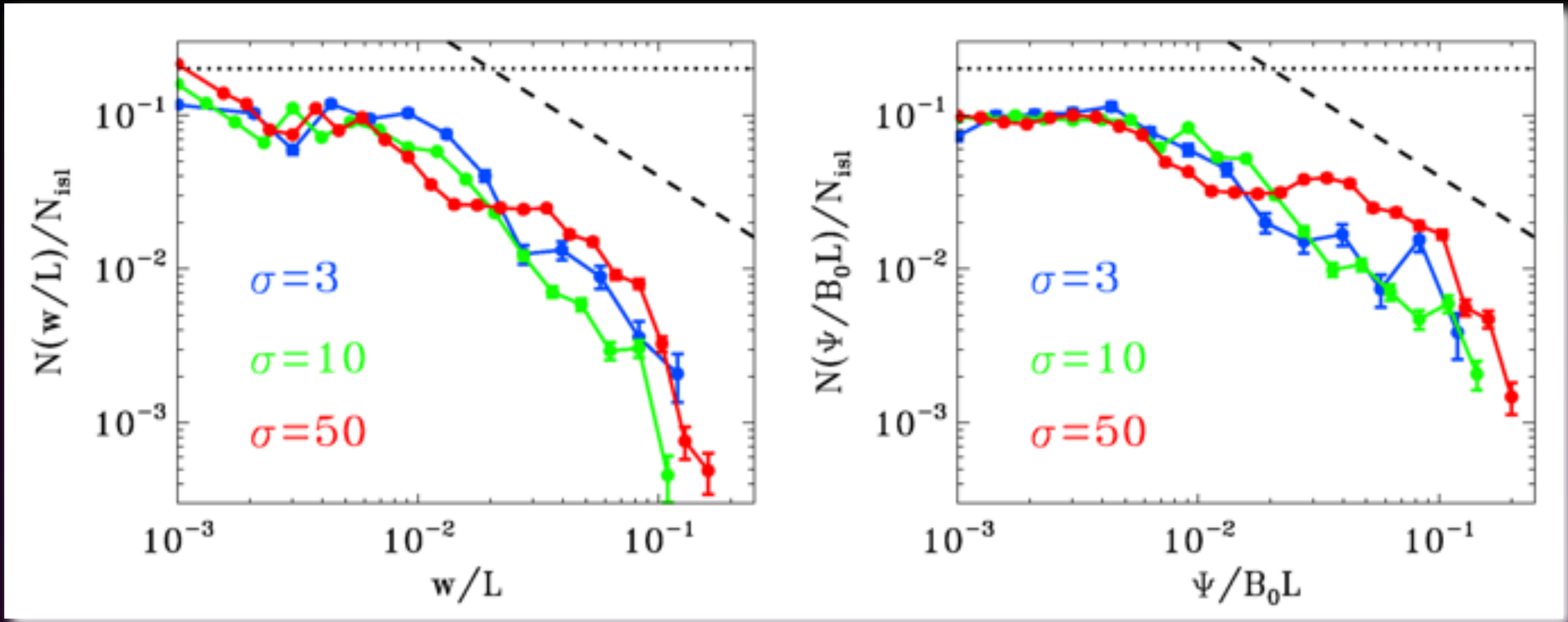

Differential distributions of magnetic flux

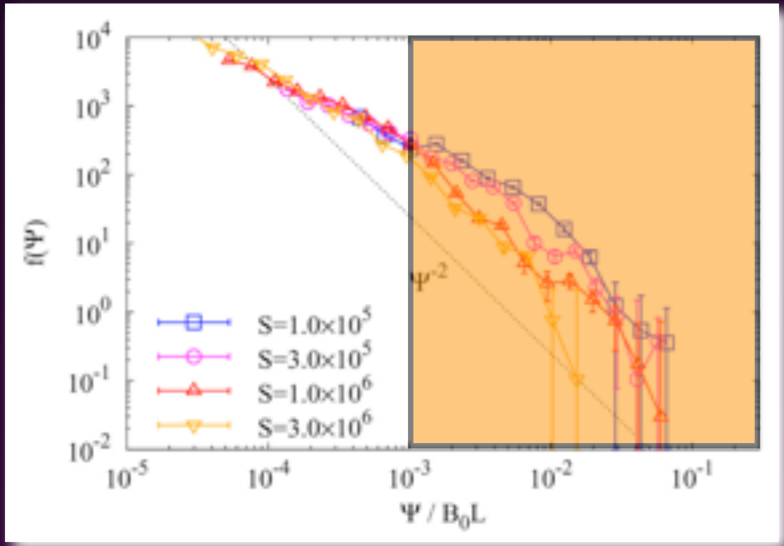

(Loureiro+12)

(Huang+12)

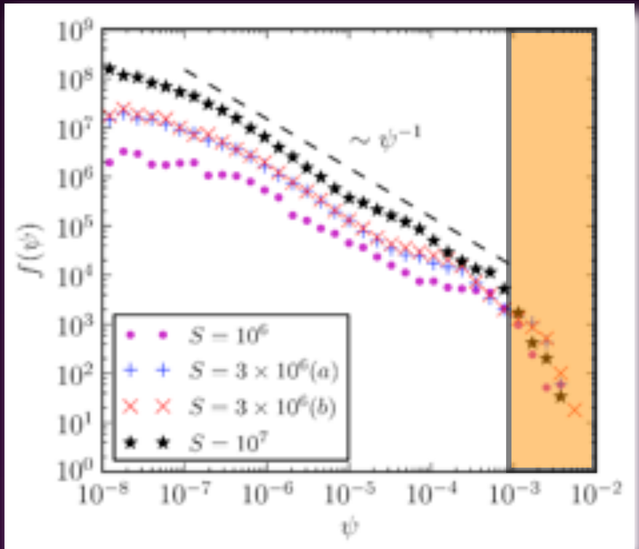

Plasmoid space-time tracks

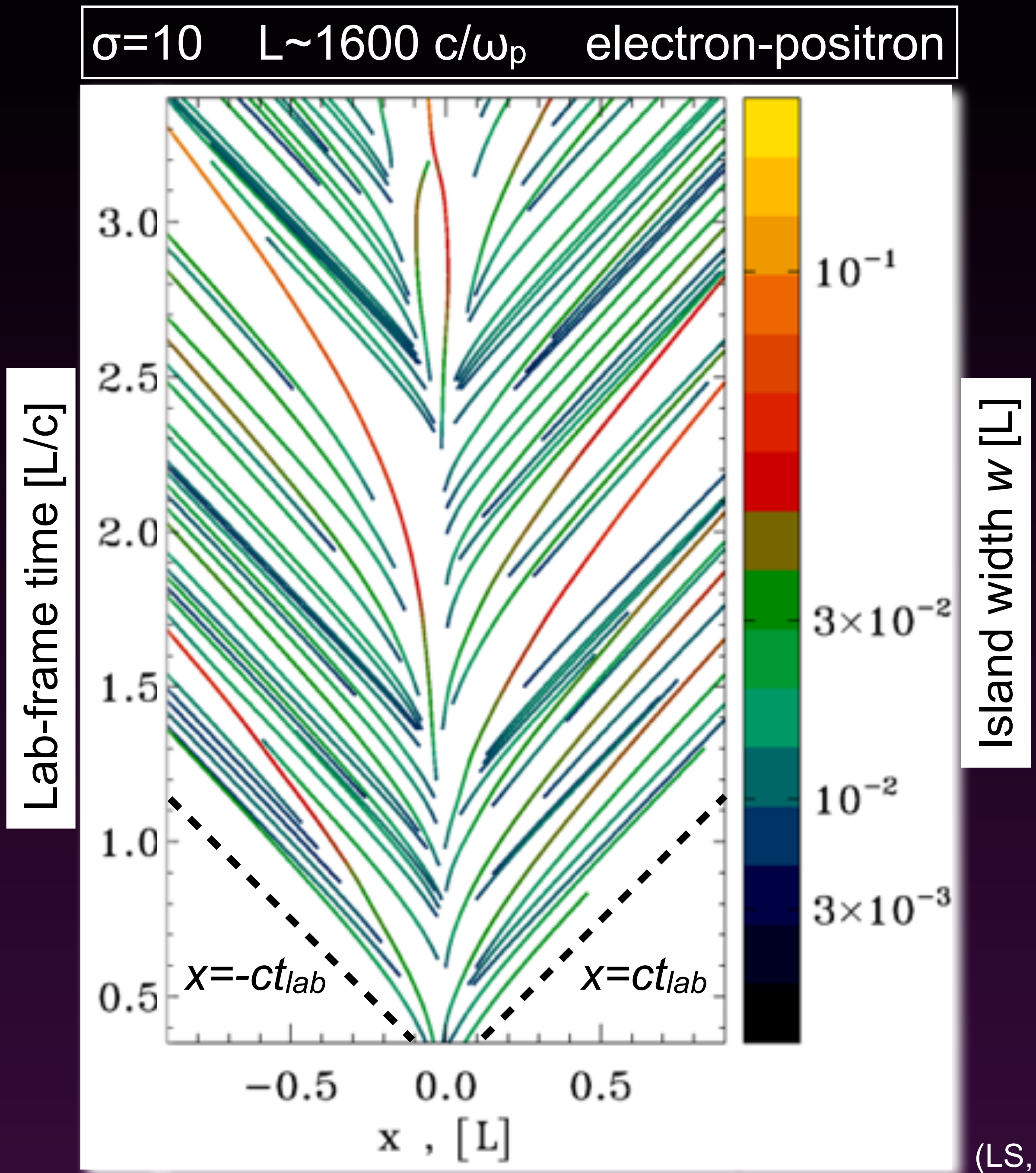

We can follow individual plasmoids in space and time.

First they grow, then they go:

- First, they grow in the center at non-relativistic speeds.
- Then, they accelerate outwards approaching the Alfven speed ~ *c*.

(LS, Giannios & Petropoulou 16)

First they grow, then they go

σ=10 electron-positron

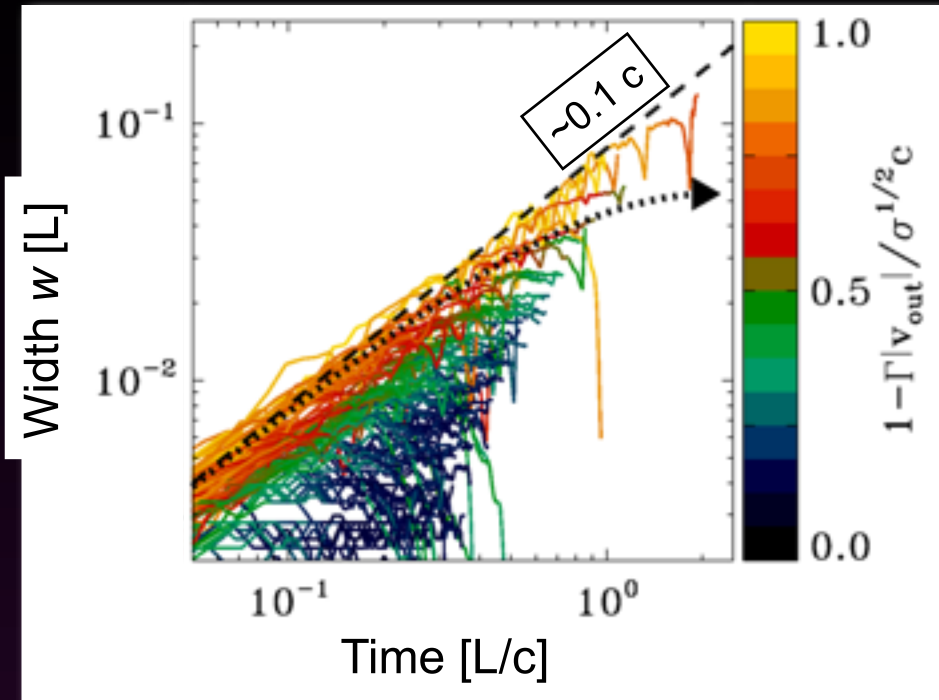

- The plasmoid width *w* grows in the plasmoid rest-frame at a constant rate of ~0.1 c (~ reconnection inflow speed), weakly dependent on the magnetization.

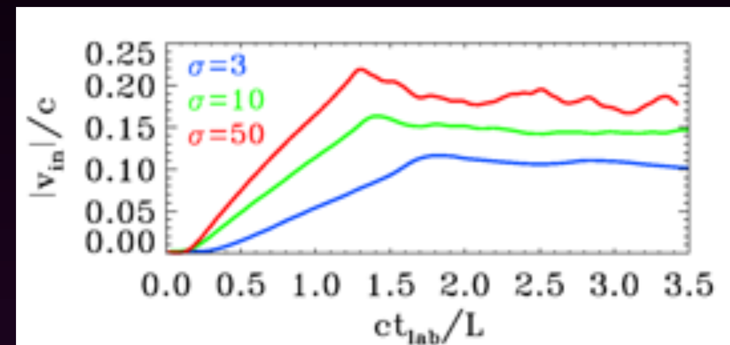

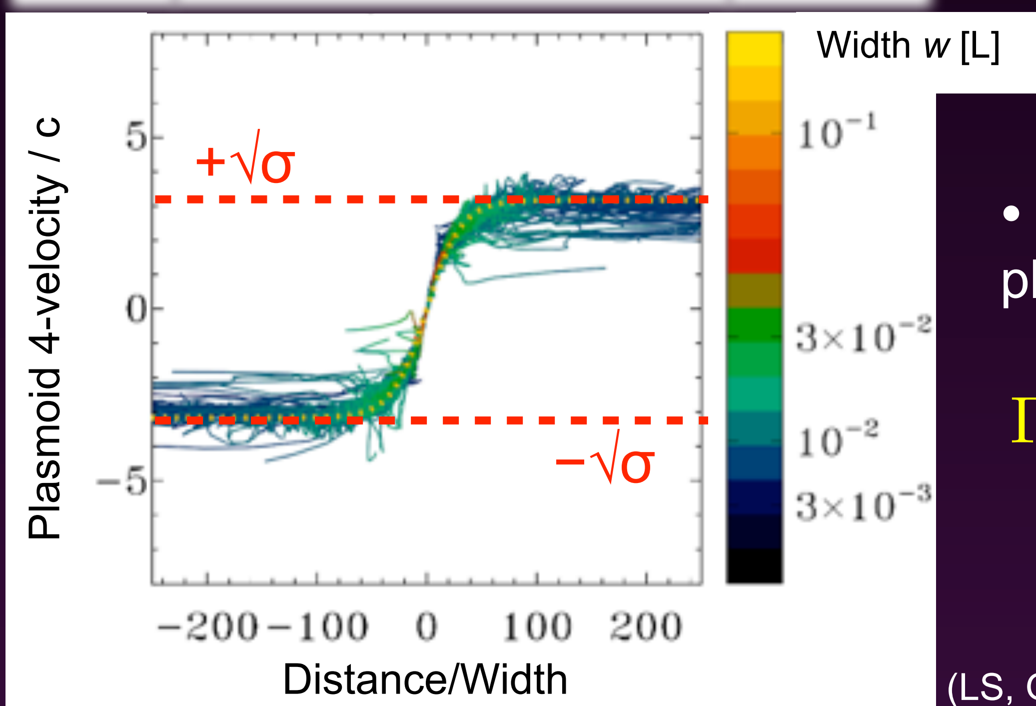

- Universal relation for the plasmoid acceleration:

$$\Gamma\frac{v_{\rm out}}{c} \simeq \sqrt{\sigma}\,\tanh\left(\frac{0.1}{\sqrt{\sigma}}\frac{x}{w}\right)$$

(LS, Giannios & Petropoulou 16)

Small is fast, large is slow

σ=10 electron-positron

(Petropoulou, Giannios & LS 16)

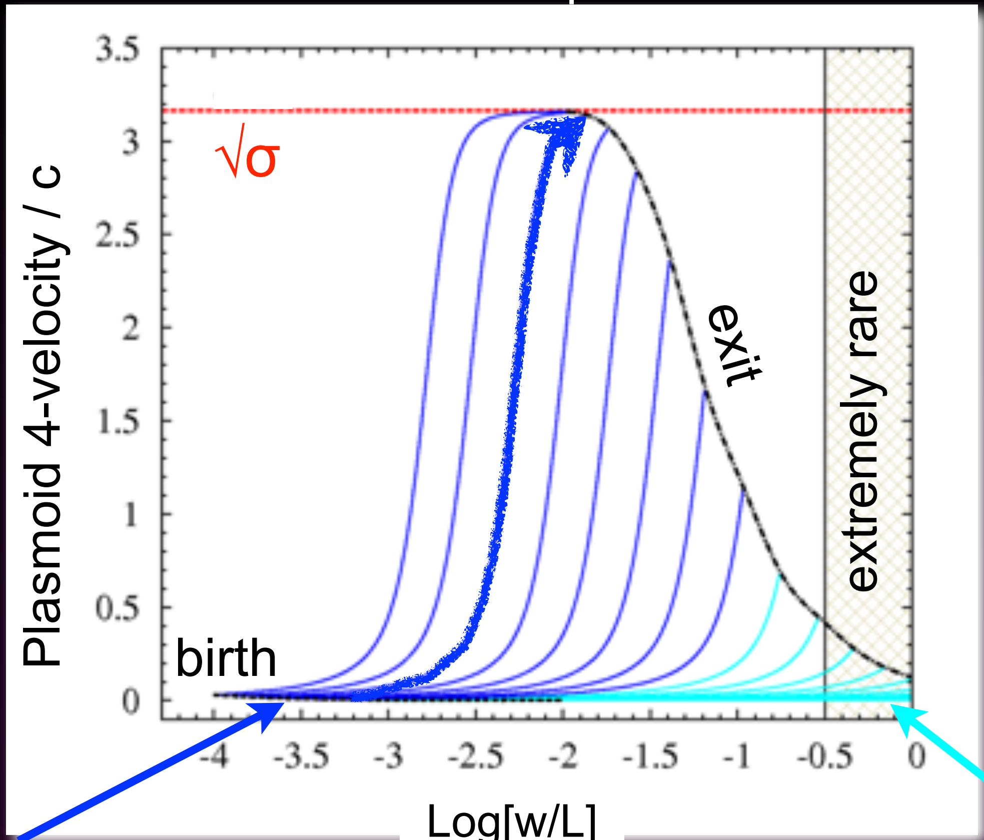

Small and fast

Large and slow

If the width at the end of the layer is

$$w_{\rm f} \lesssim w_{\rm f,\sqrt{\sigma}} \sim 0.03 \frac{L}{\sqrt{\sigma_1}}$$

the plasmoid will exit the layer with 4-velocity →√σ *c*.

If the width at the end of the layer is

$$w_{\rm f} \gtrsim w_{\rm f,c} \sim 0.1\, L$$

the plasmoid will exit the layer still non-relativistic.

From microscoPIC to MHD scales

Let us measure the system length L in units of the post-reconnection Larmor radius:

$$r_{0,\mathrm{hot}} = \sigma \frac{mc^2}{eB_0}$$

σ=10 electron-positron

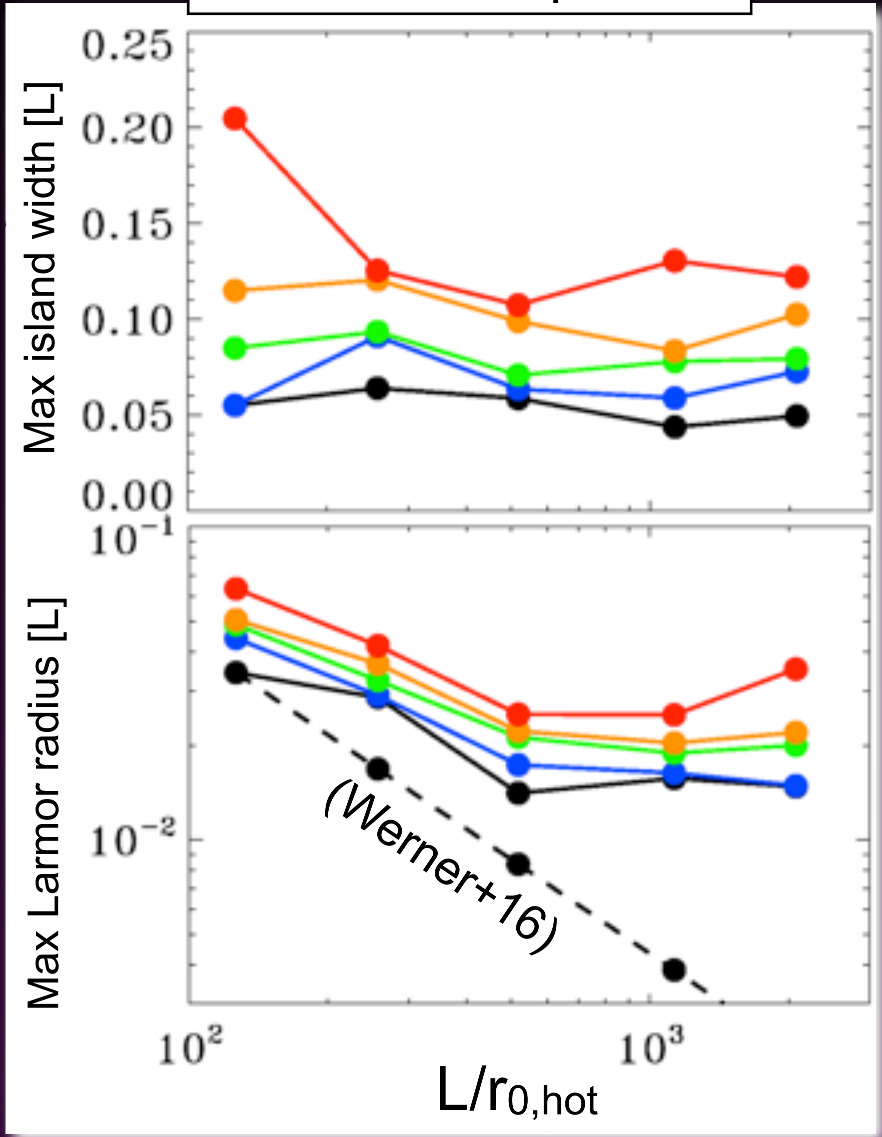

Relativistic reconnection is a self-similar process, in the limit $L \gg r_{0,\mathrm{hot}}$:

- The width of the biggest ("monster") islands is a fixed fraction (~0.1-0.2) of the system length L.

- The Larmor radius of the highest energy particles is a fixed fraction (~0.03-0.05) of the system length L.

→ the scaling extrapolates up to MHD scales.

(LS, Giannios & Petropoulou 16)

Particle anisotropy from PIC to MHD scales

σ=10 electron-positron

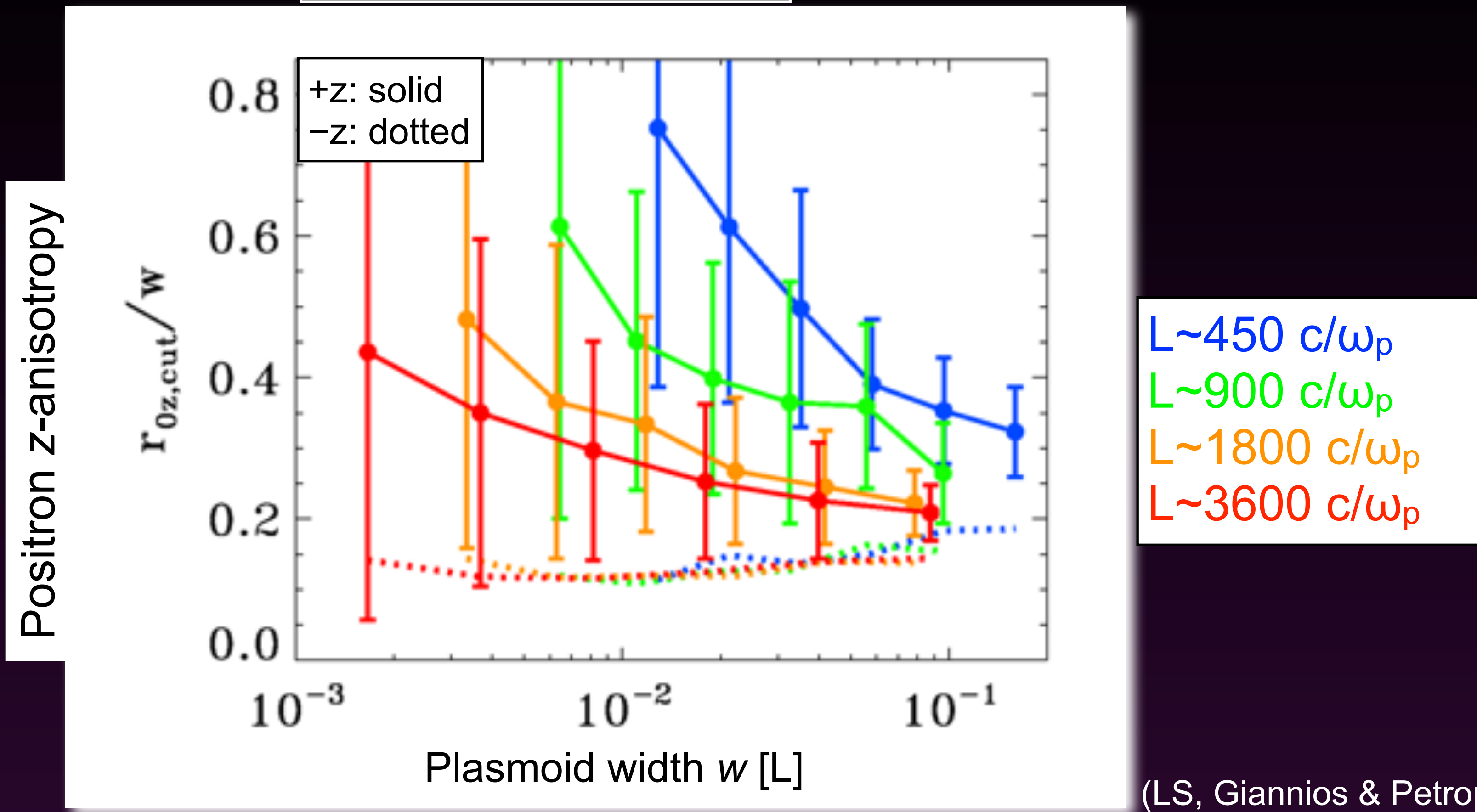

(LS, Giannios & Petropoulou 16)

- Small islands show anisotropy along *z* (along the reconnection electric field).

Large islands are nearly isotropic, as assumed in the MHD description!

The transition happens at $w \sim 50\sqrt{\sigma}\, c/\omega_{\rm p}$

Monte Carlo modeling of plasmoid statistics

In blazars, the emission scale is 9 orders of magnitude larger than the skin depth!

One possible strategy:

- extract physical laws from large-scale PIC simulations.
- develop a Monte Carlo code that follows the evolution of individual plasmoids as they grow, accelerate, merge, and leave the layer.

Size distribution
(benchmarked with PIC)

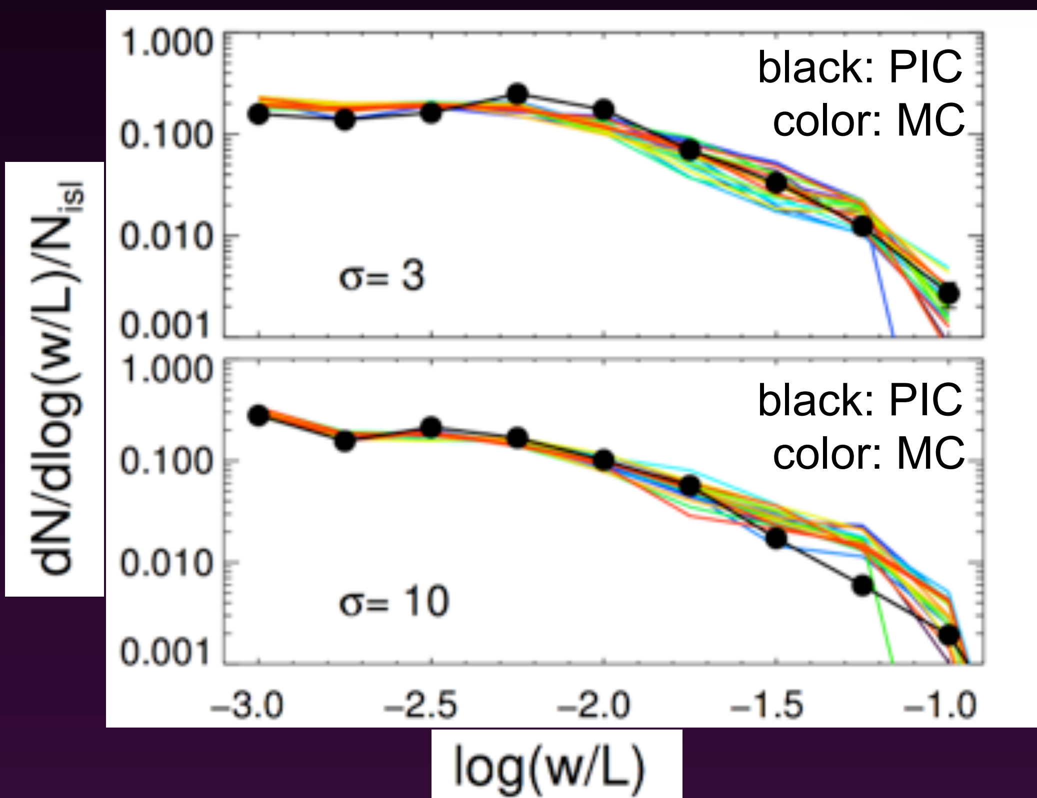

4-velocity distribution
(prediction!)

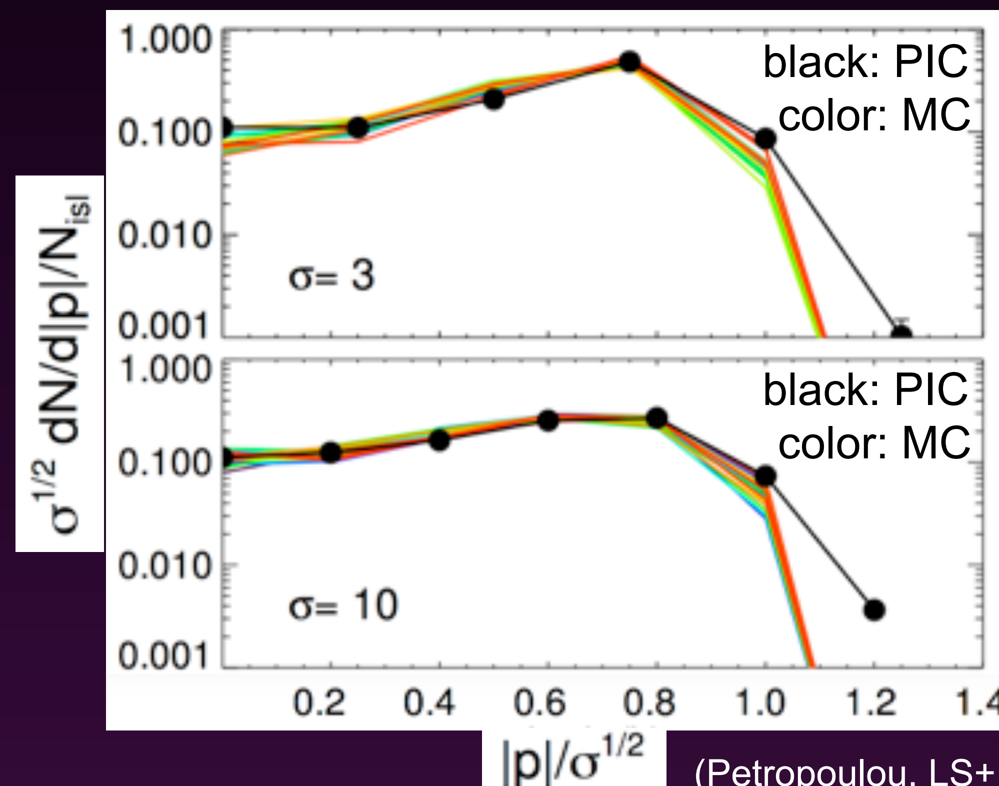

(Petropoulou, LS+ 17, any day now)

Bridging the separation of scales

With MC, we achieve more extreme separation between plasma scales and system size.

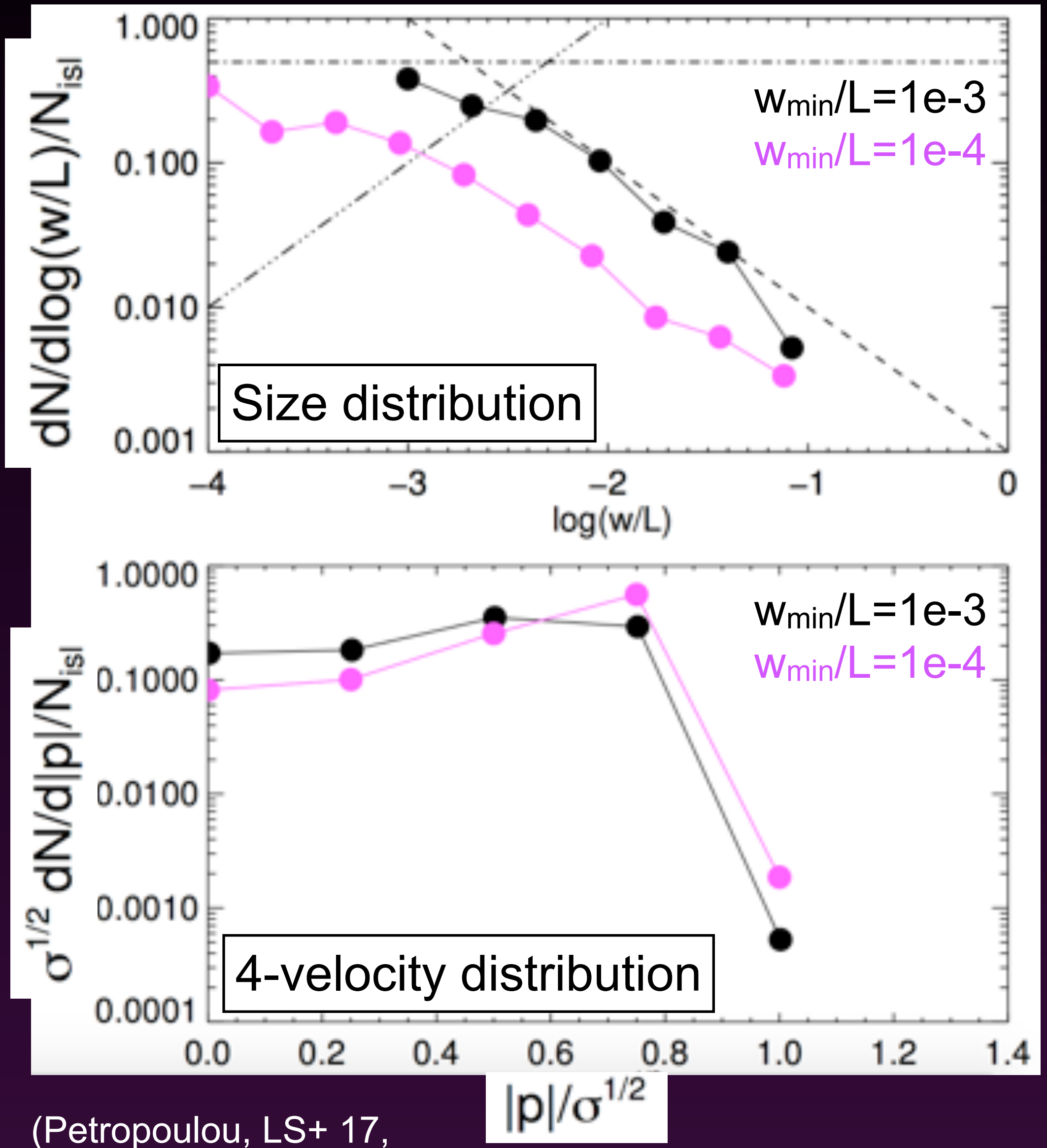

The size distribution extends to smaller sizes, but at larger sizes it stays the same (apart from an overall normalization).

The 4-velocity distribution is nearly unchanged.

(Petropoulou, LS+ 17, any day now)

Light curves and SED

$\sigma=10 \quad \theta_{obs}=0.5/\Gamma_j$

Rise: based on PIC simulations.

Decay: parameterized (cooling / photon diffusion / drop in particle injection).

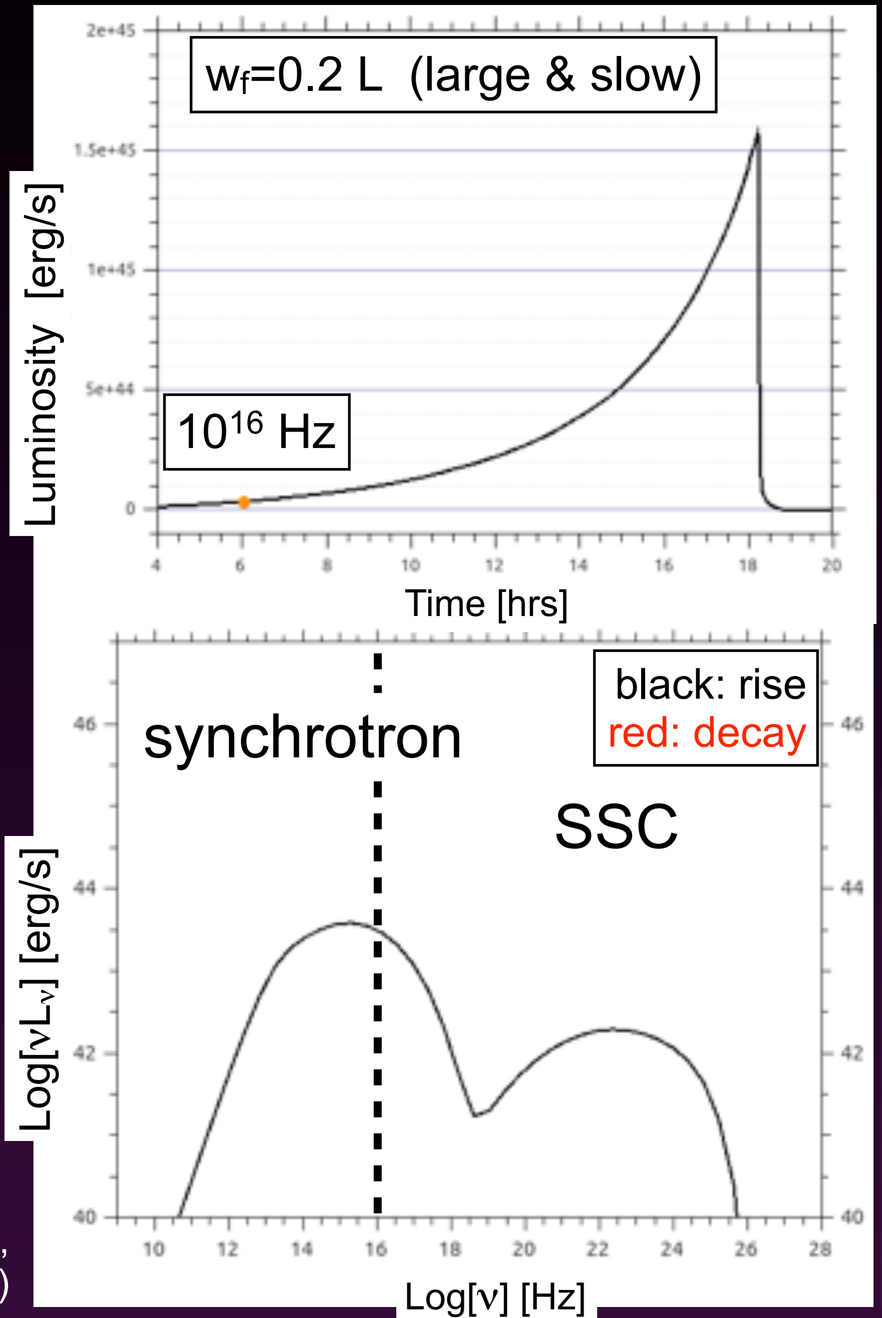

(Petropoulou, Giannios & LS 16)

3C 279

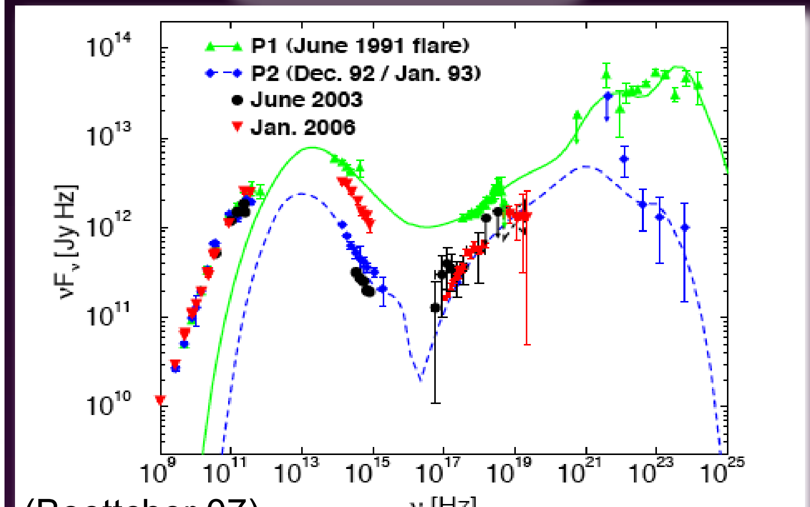

(Boettcher 07)

Light curves and SED

$\sigma=10 \quad \theta_{obs}=0.5/\Gamma_j$

Rise: based on PIC simulations.

Decay: parameterized (cooling / photon diffusion / drop in particle injection).

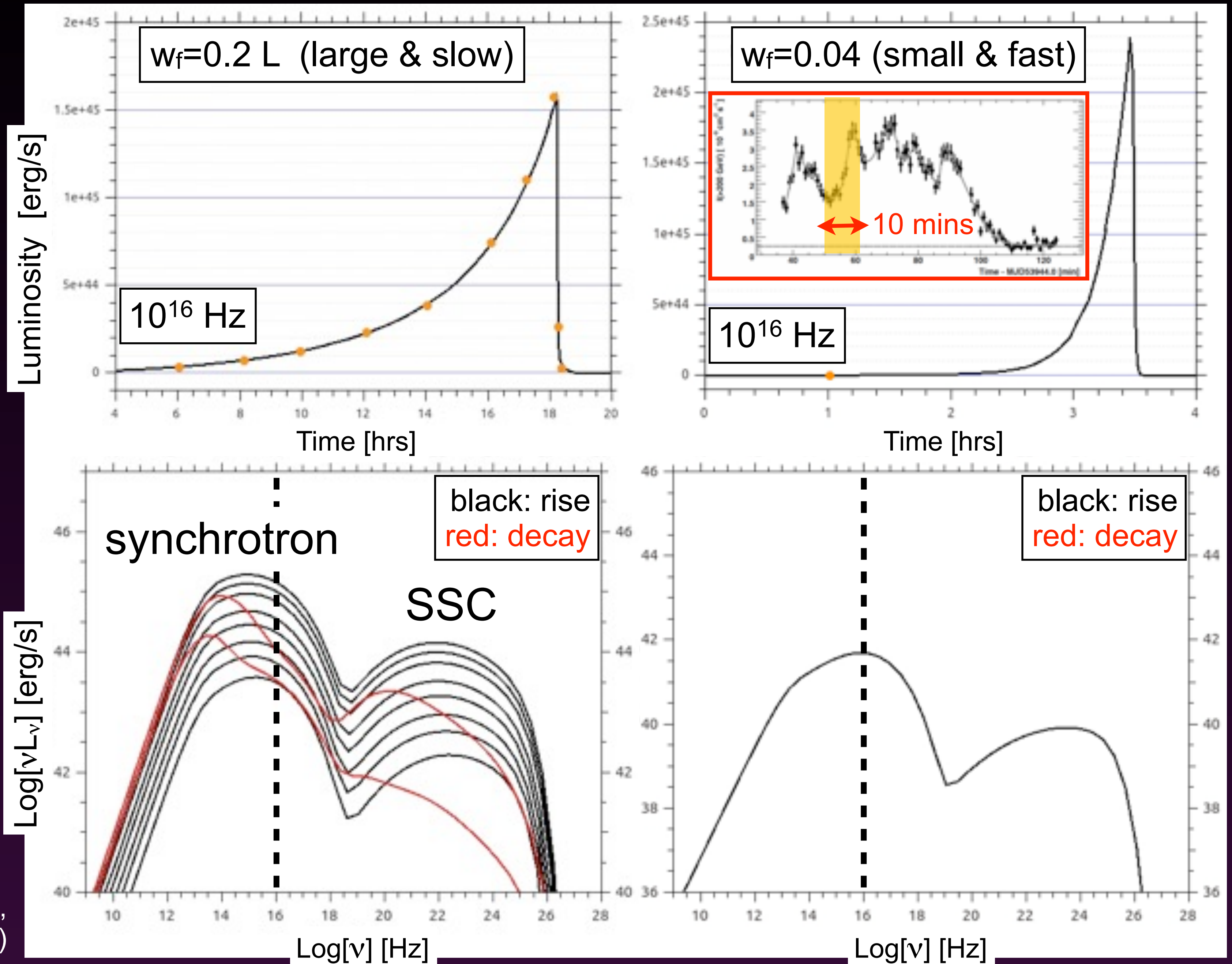

(Petropoulou, Giannios & LS 16)

2. Reconnection in accretion disks

Sgr A*

Sgr A* : expected image

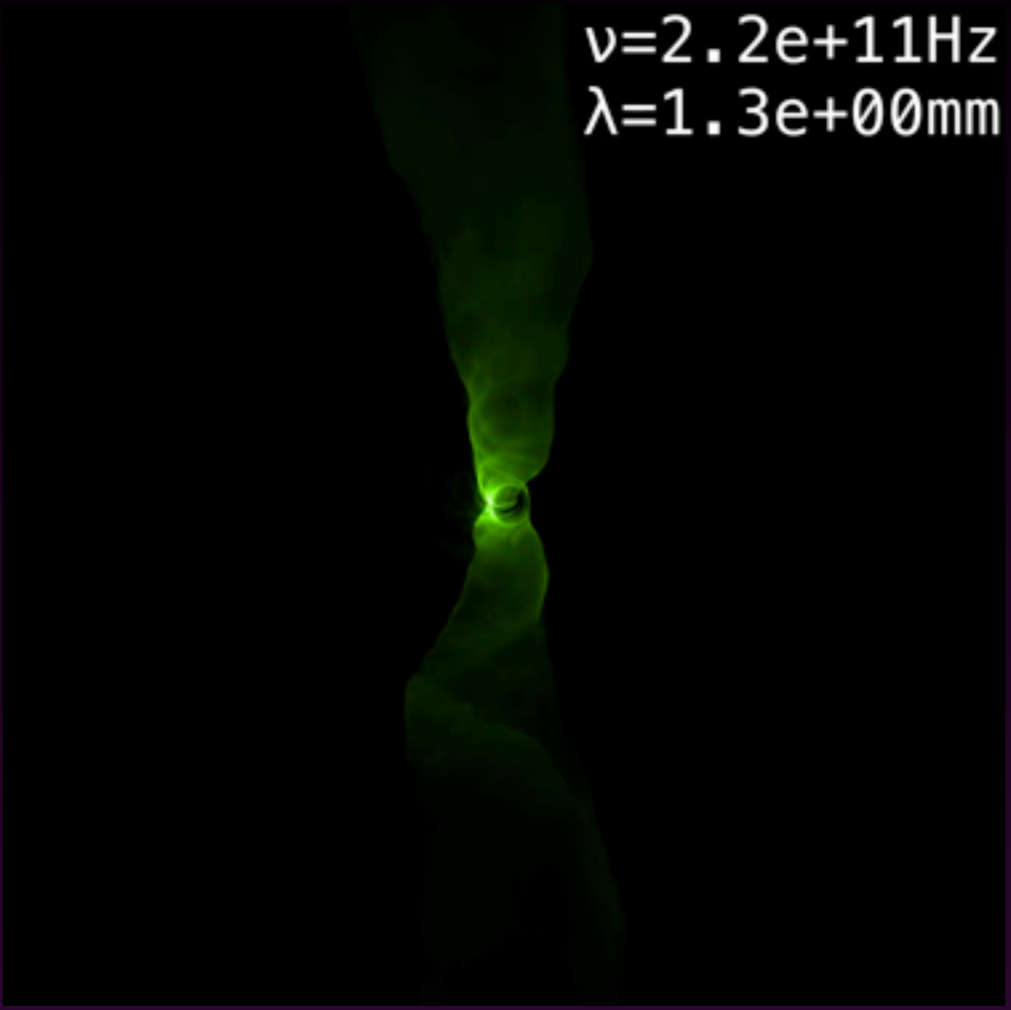

(Event Horizon Telescope)

Sgr A* : spectrum

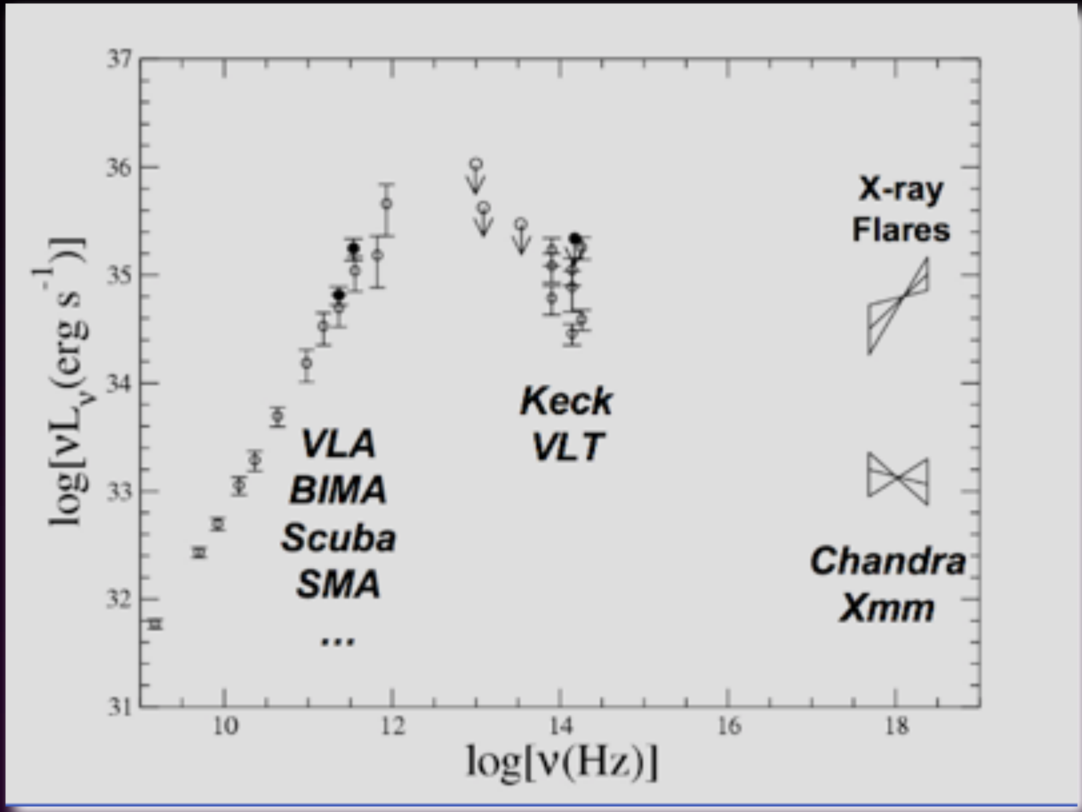

- Reconnection has been invoked to explain the spectrum and time variability of the X-ray flares from Sgr A* (e.g., Ponti+ 17)

Reconnection in Sgr A*

Sgr A* : GRMHD simulations

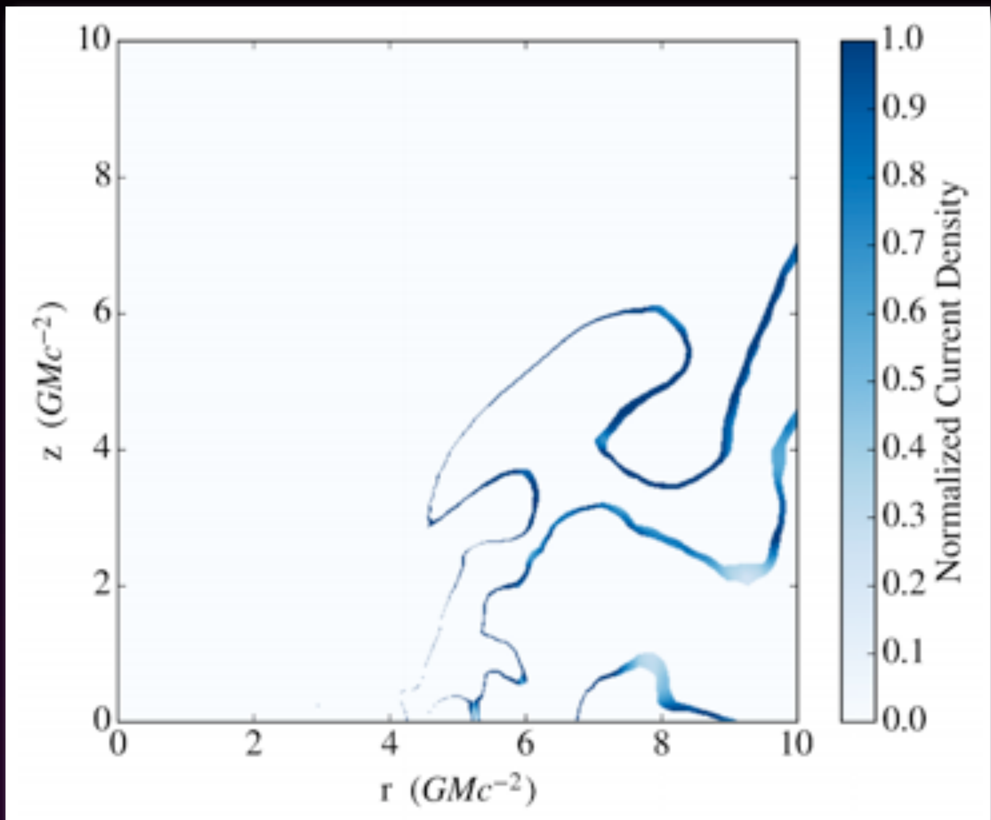

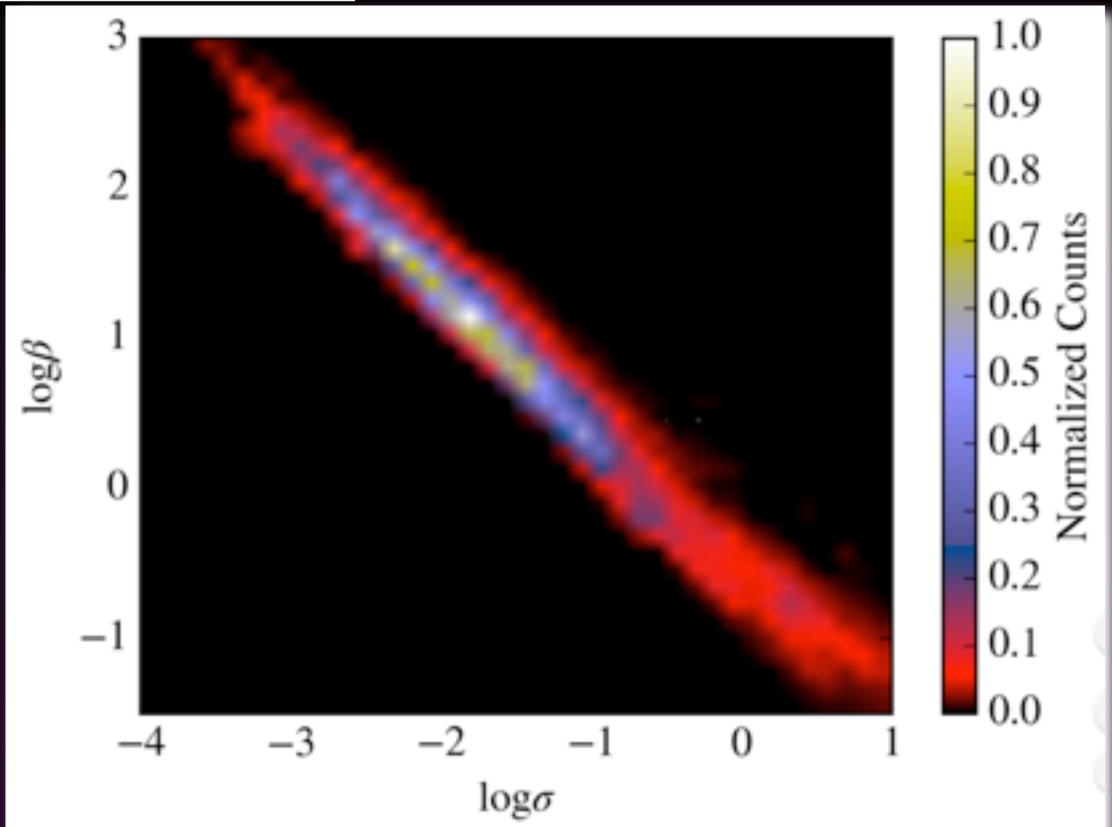

(Ball+ 17)

- Reconnection current sheets appear in GRMHD simulations of low-luminosity accretion flows.

- The plasma around reconnection layers spans a range of beta and sigma.

$$\beta = \frac{8\pi n_0 k_B T}{B_0^2} \qquad \sigma = \frac{B_0^2}{4\pi n_0 m_p c^2}$$

Dependence on beta

σ=0.1 β=0.01

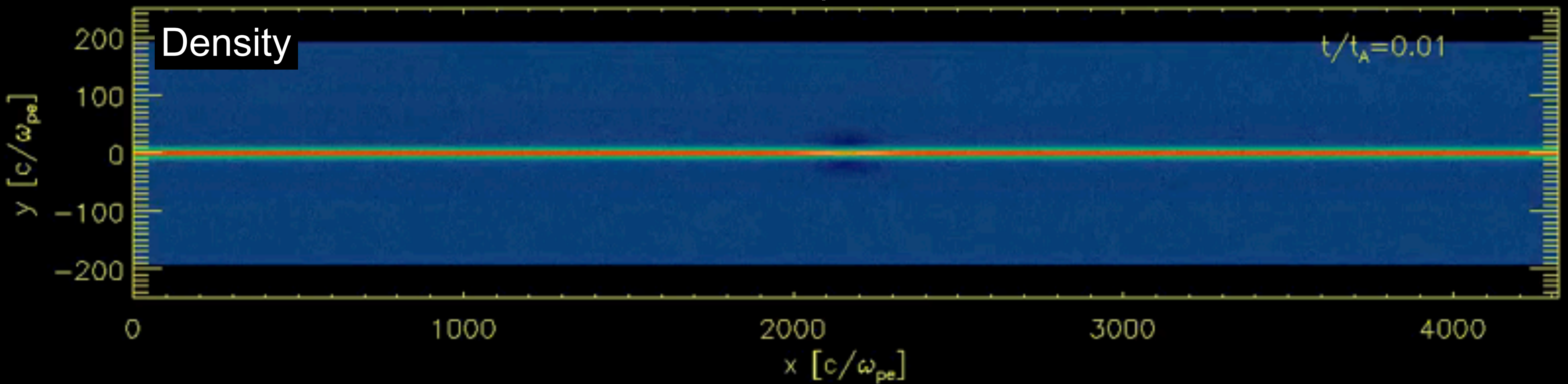

σ=0.1 β=2

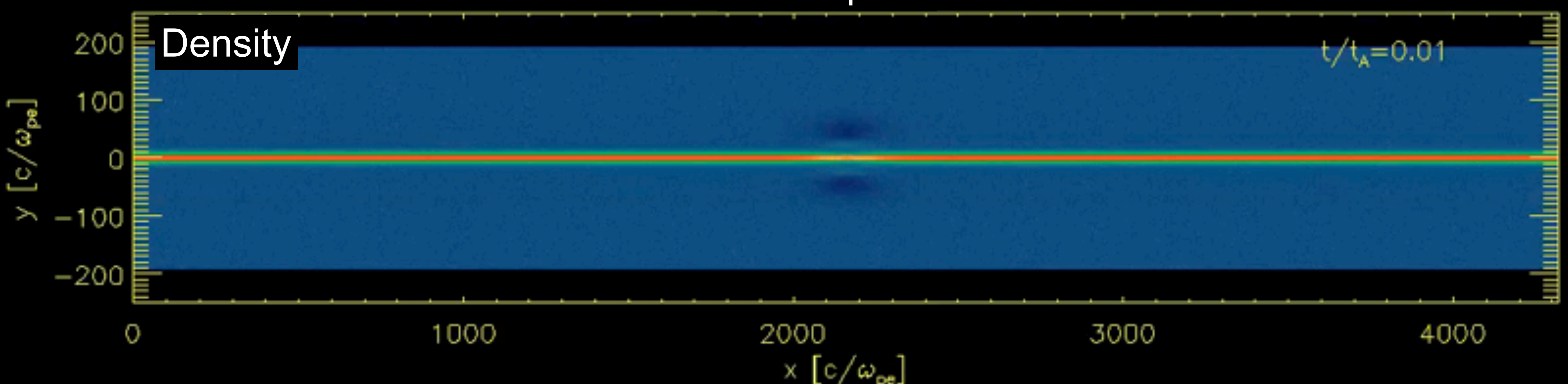

(Rowan, LS & Narayan 2017)

Dependence on beta

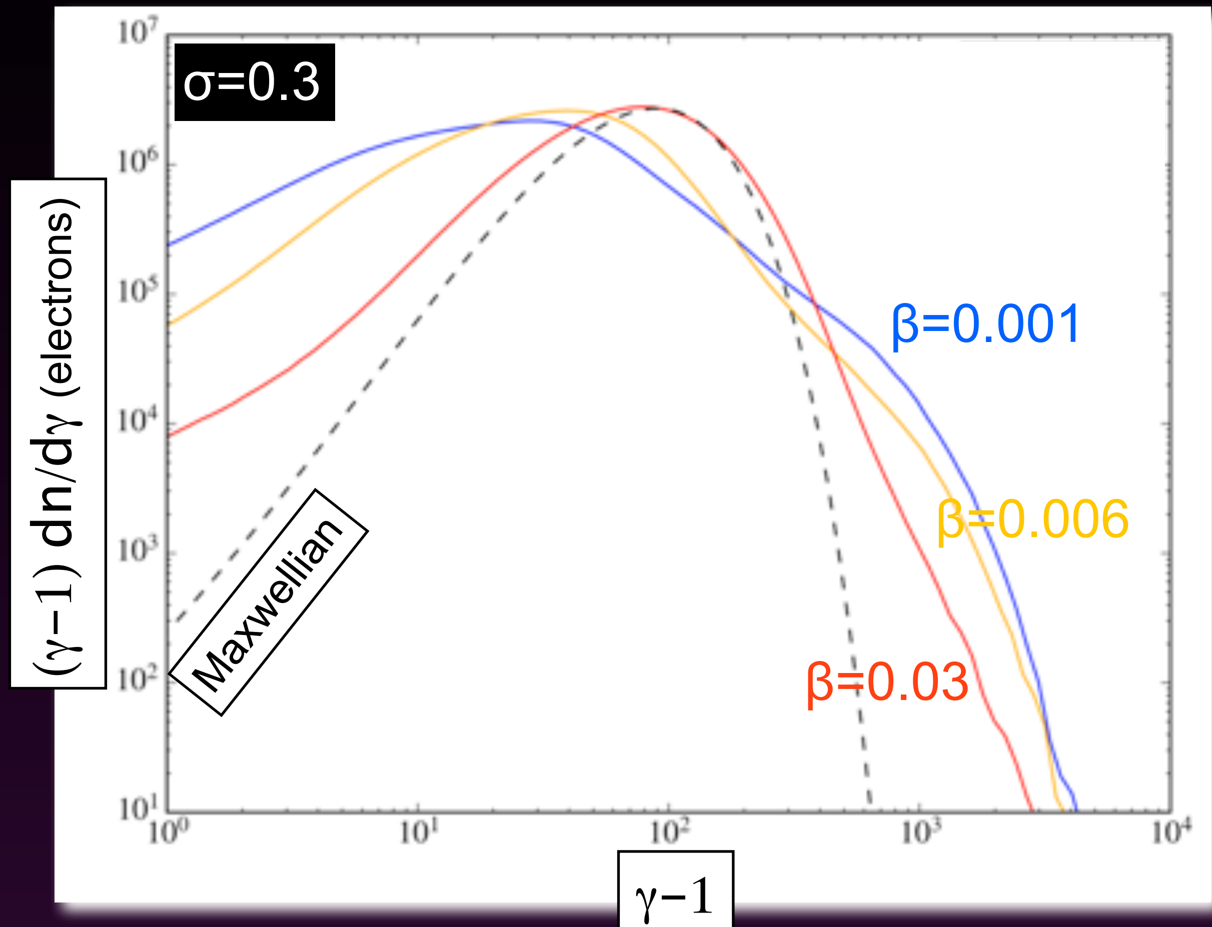

(Ball & LS, in prep)

- Low beta: fragmentation into secondary plasmoids, hard electron spectra.
- High beta: smooth layer, steep electron spectra (nearly Maxwellian).

Dependence on beta and sigma

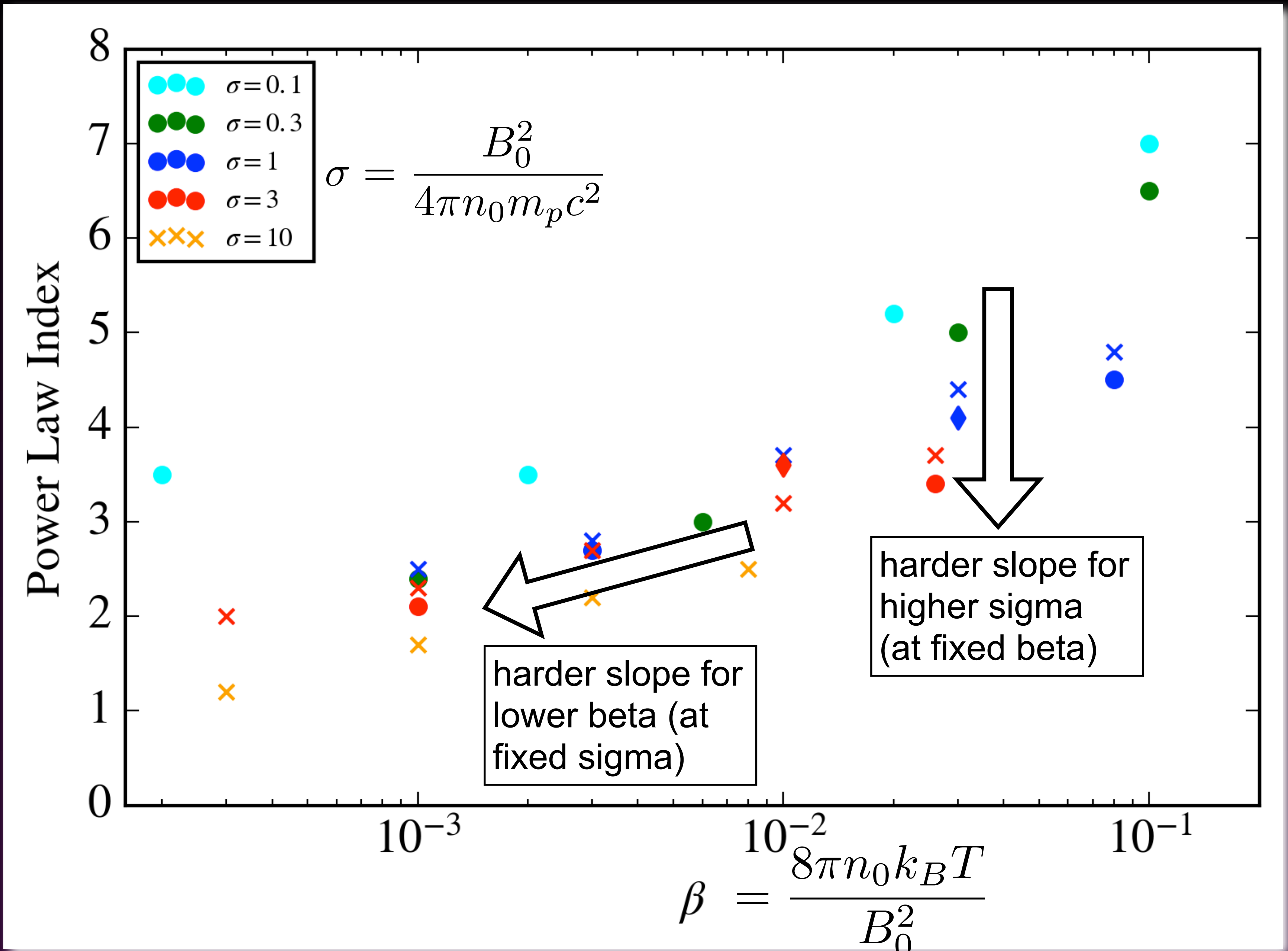

(Ball & LS, in prep)

Particle acceleration mechanism

The highest energy electrons

2D σ=0.3 electron-proton

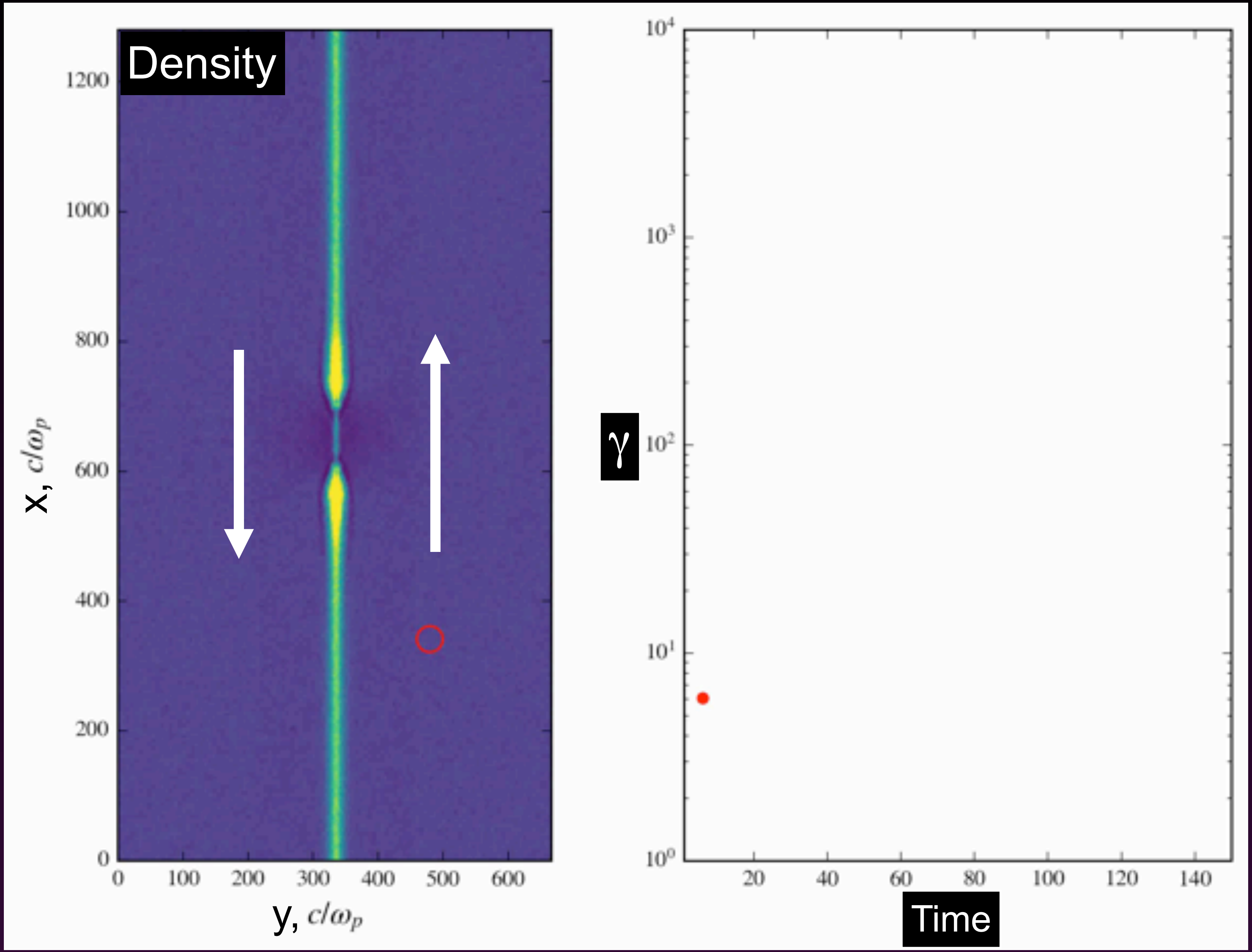

(Ball & LS, in prep)

Two acceleration phases: (a) at the X-point; (b) in between merging islands

The highest energy particles

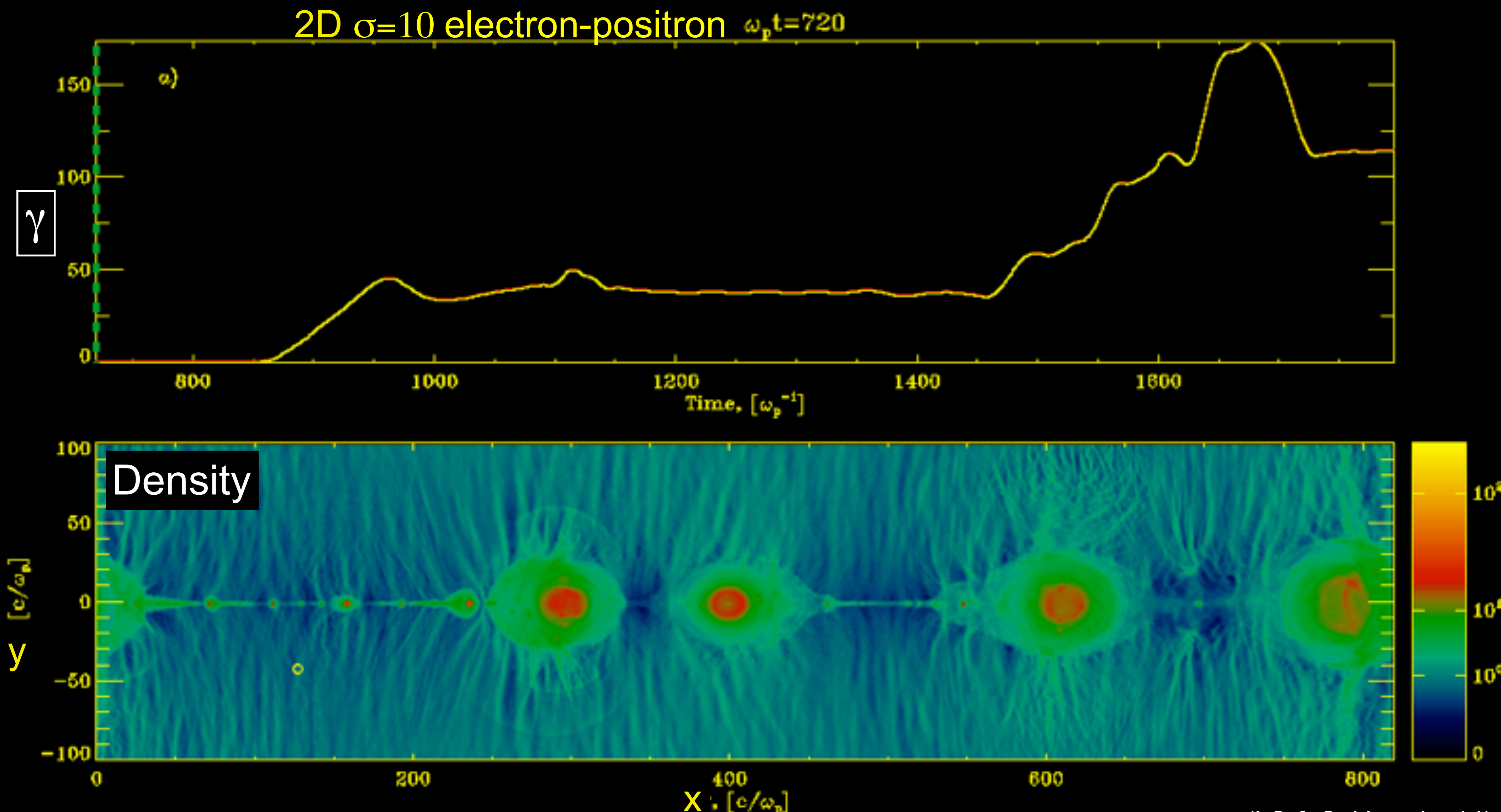

(LS & Spitkovsky 14)

Two acceleration phases: (a) at the X-point; (b) in between merging islands

(b) Fermi process in between islands

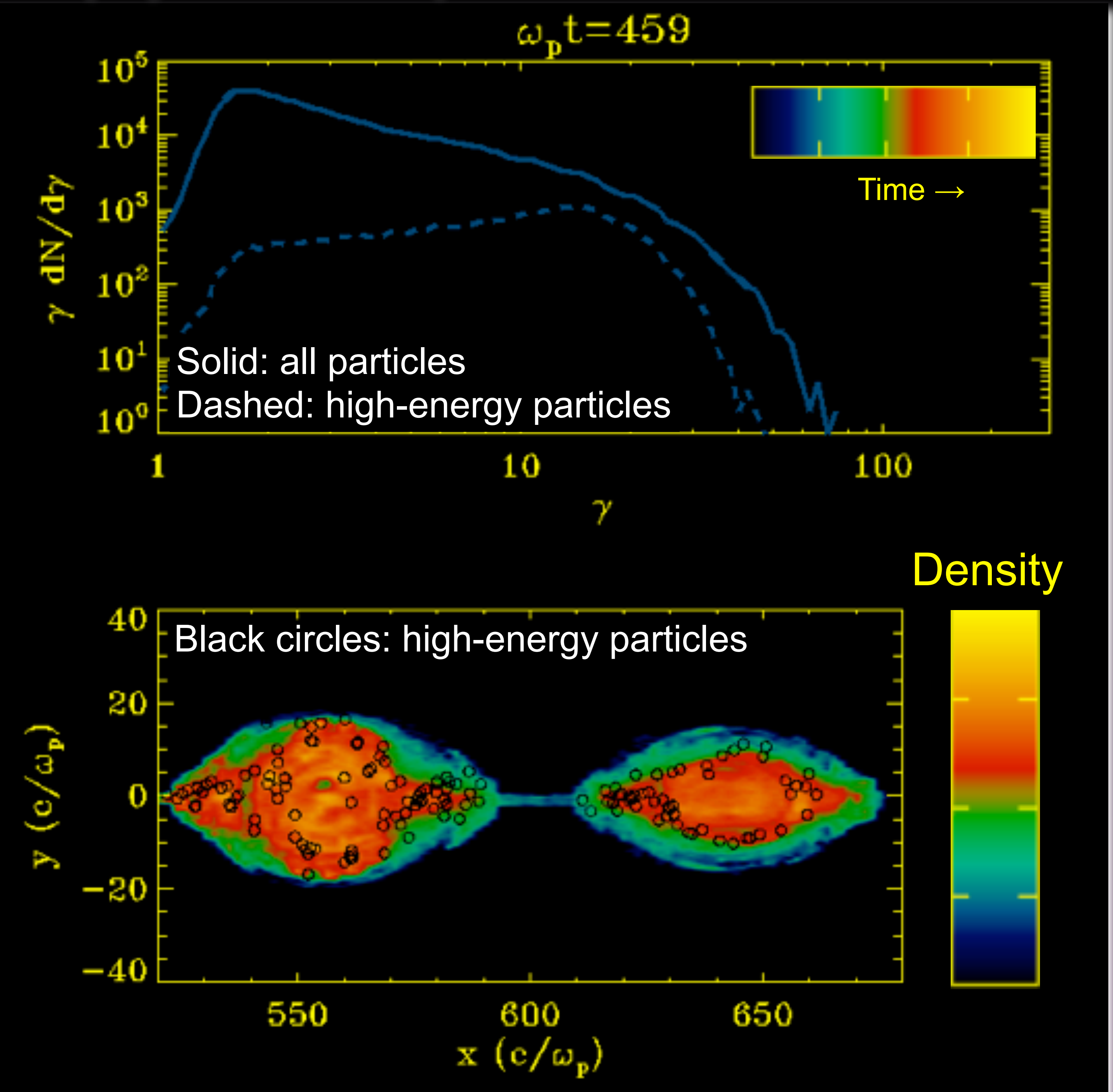

- The particles are accelerated by a Fermi-like process in between merging islands (Guo+14, Nalewajko+15).

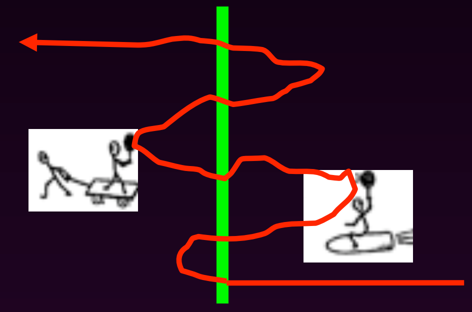

- Island merging is essential to shift up the spectral cutoff energy.

- In the Fermi process, the rich get richer. But how do they get rich in the first place?

(a) Acceleration at X-points

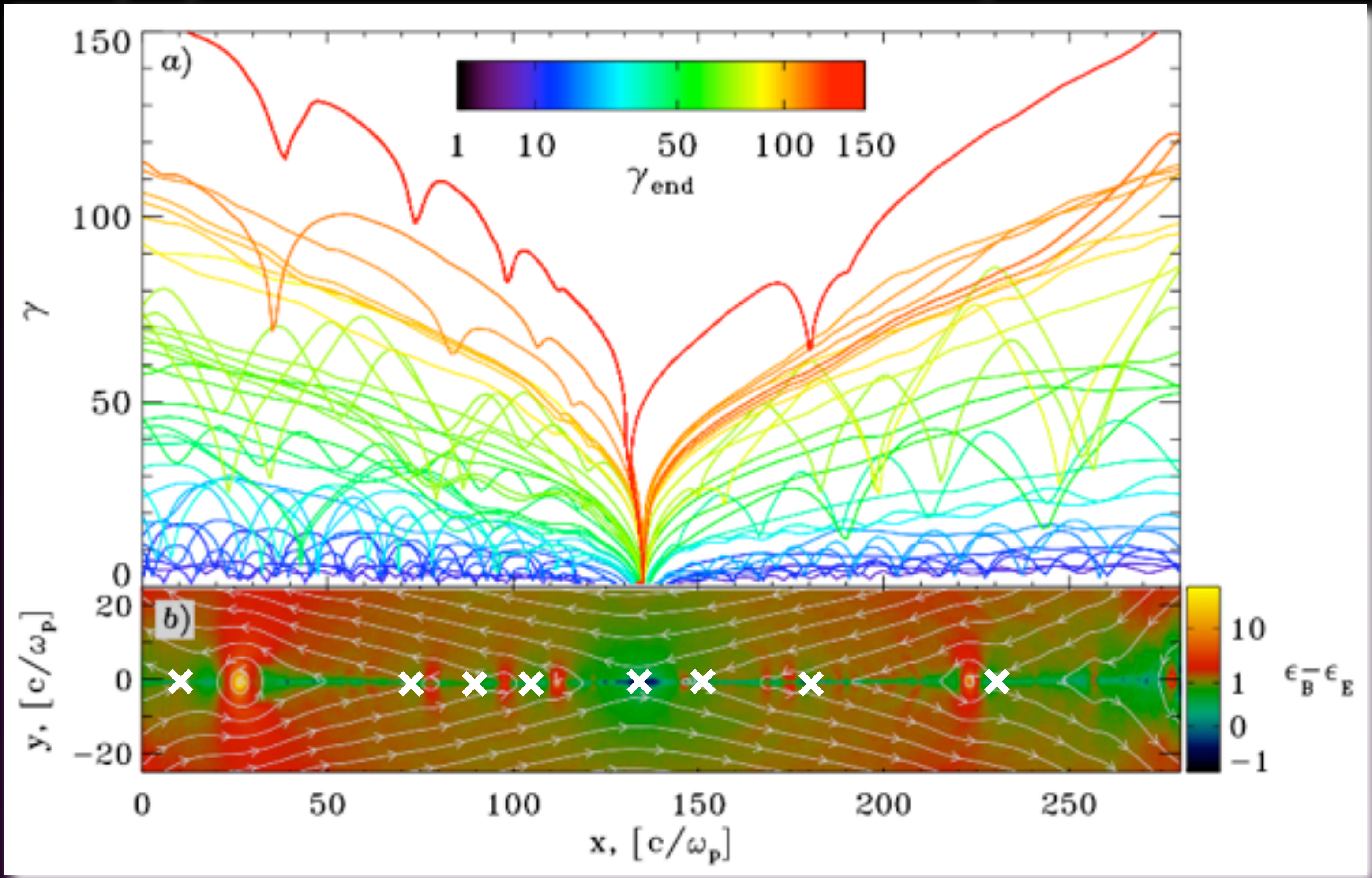

(LS & Spitkovsky 14)

- In cold plasmas, the particles are tied to field lines and they go through X-points.
- The particles are accelerated by the reconnection electric field at the X-points (Zenitani & Hoshino 01). The energy gain can vary, depending on where the particles interact with the sheet.
- The same physics operates at the main X-point and in secondary X-points.

Particle injection in reconnection

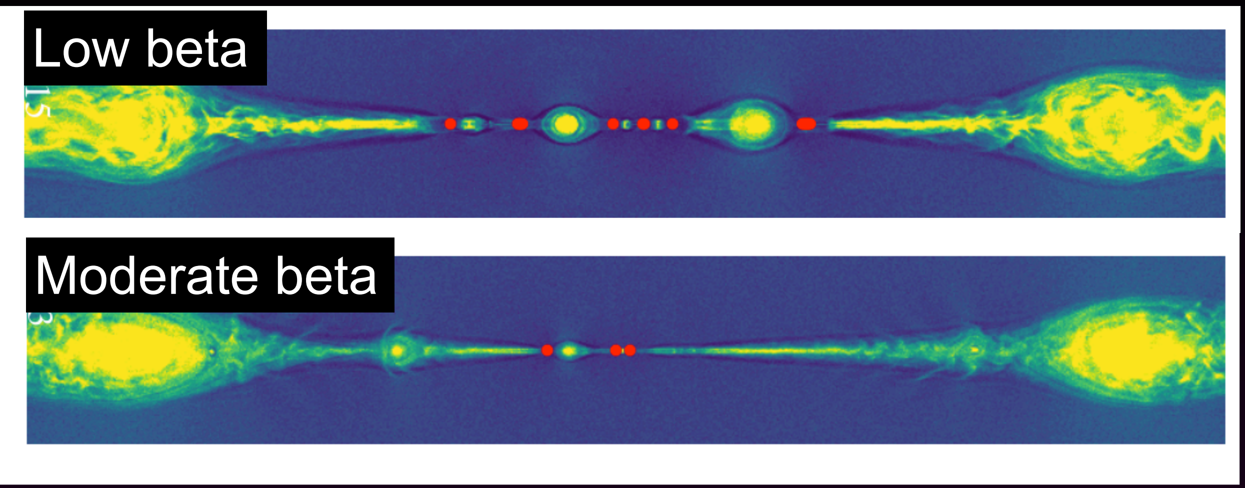

- Many more X-points (E>B) in low beta than in high beta.

X-point statistics

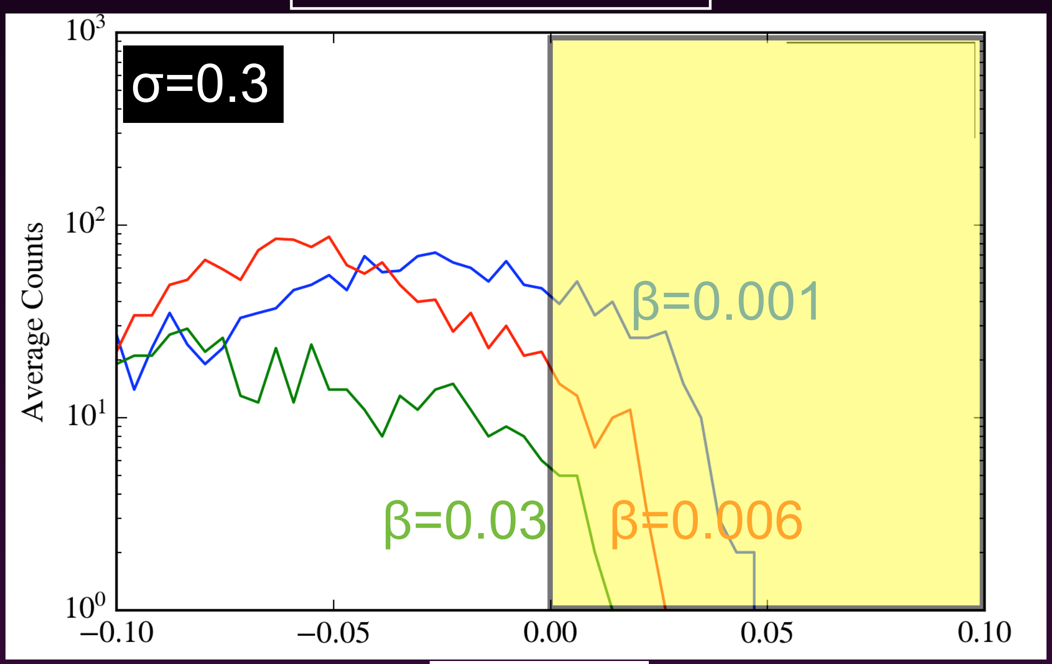

(Ball & LS, in prep)

(E-B)/B_0

1. Electron injection happens at X-points (E>B).

2. More X-points for lower beta.

3. Acceleration is more efficient / harder slopes at lower beta.

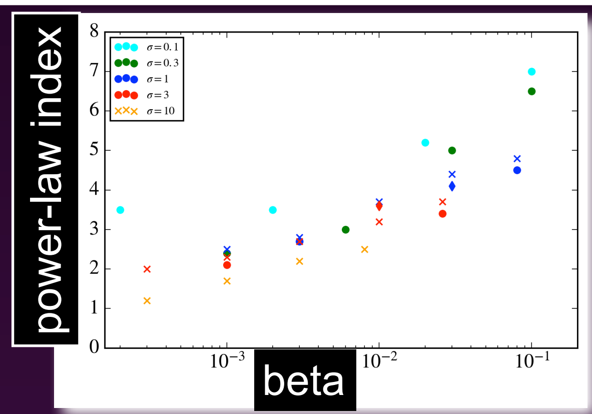

3. Reconnection in strong radiation fields

Inverse Compton in reconnection

The particles scatter off a prescribed isotropic photon field in the Thomson regime:

$$P_{IC} = \frac{4}{3}\sigma_T c \gamma^2 U_\star$$

In the ultra-relativistic limit, the Compton drag force is

$$\vec{f} = -P_{IC}\frac{\vec{v}}{c^2}$$

We parameterize the radiation energy density via a critical Lorentz factor γ_{cr} (balancing acceleration with IC losses):

$$eEc \sim \frac{4}{3}\sigma_T c \gamma_{cr}^2 U_\star \qquad\qquad E \sim 0.1B$$

Weak IC losses

No difference in the inflow speed, outflow 4-velocity or plasmoid energy content.

The high-energy cutoff of the particle spectrum recedes to lower energies.

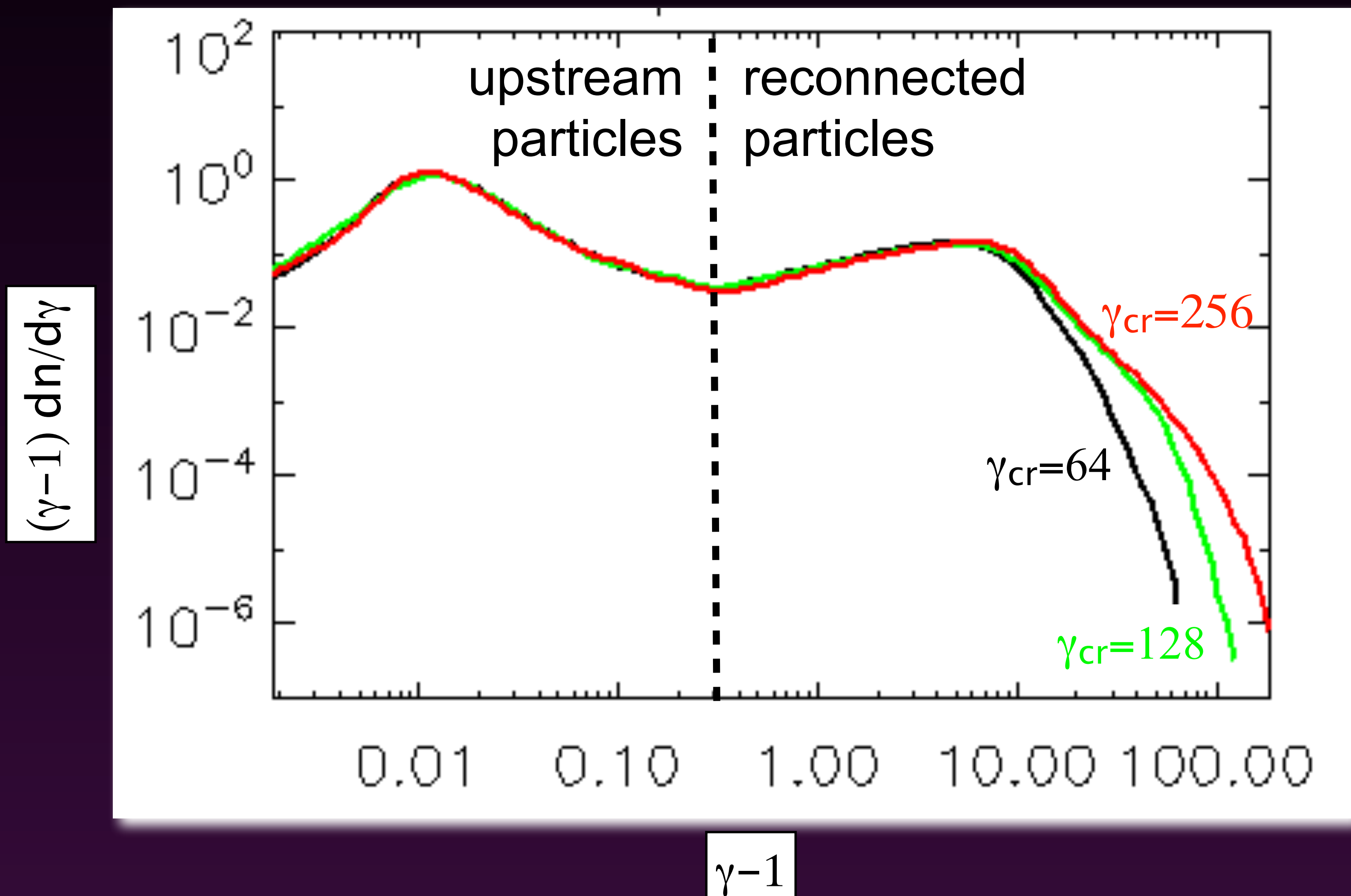

(LS & Beloborodov 17, in prep)

Moderate IC losses

No difference in the inflow speed and maximum outflow 4-velocity.

Effect of Compton drag depends on plasmoid size
(small plasmoids are unaffected; intermediate plasmoids are decelerated).

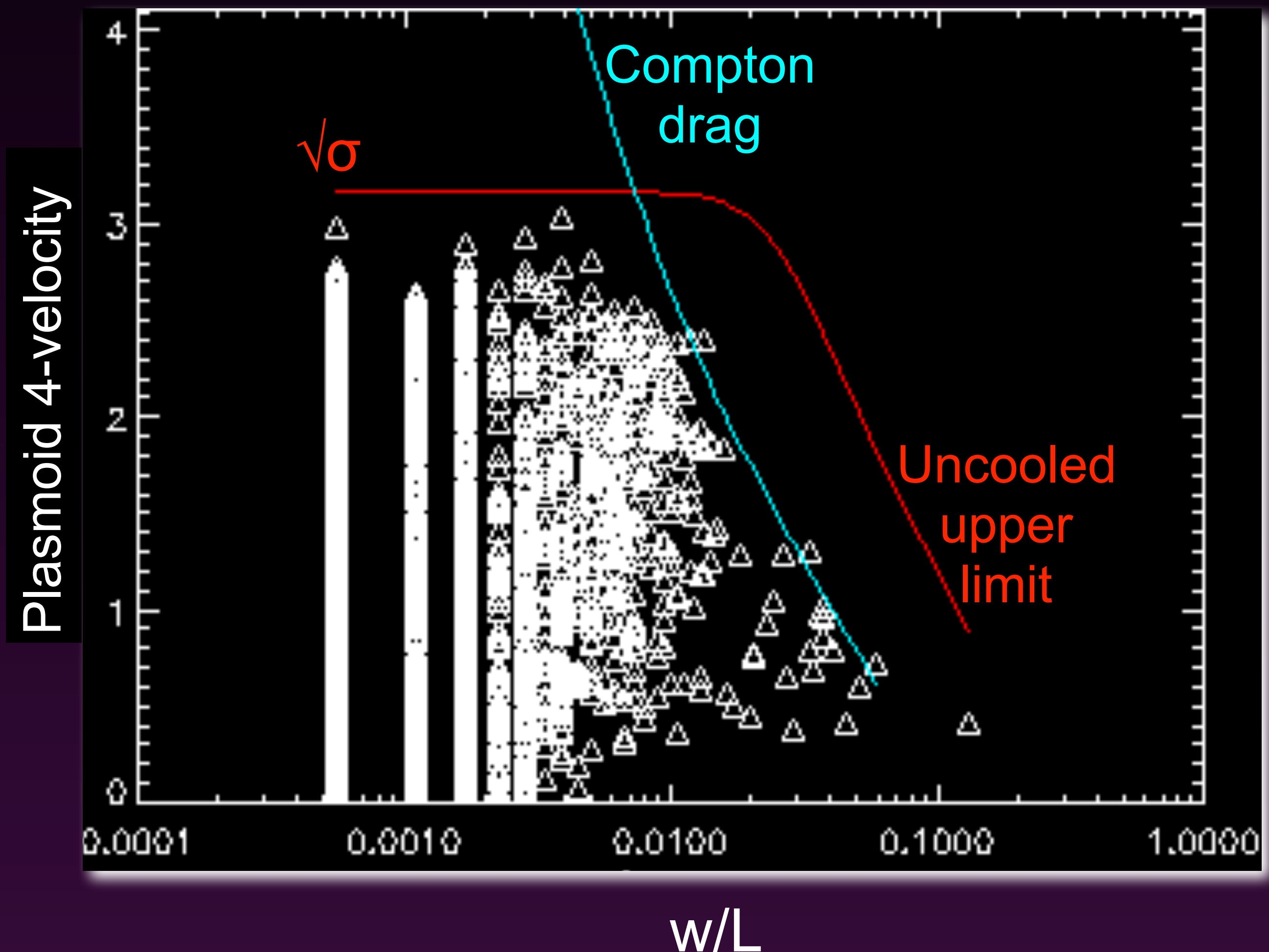

Strong IC losses

No cooling

$\gamma_{cr}=8$

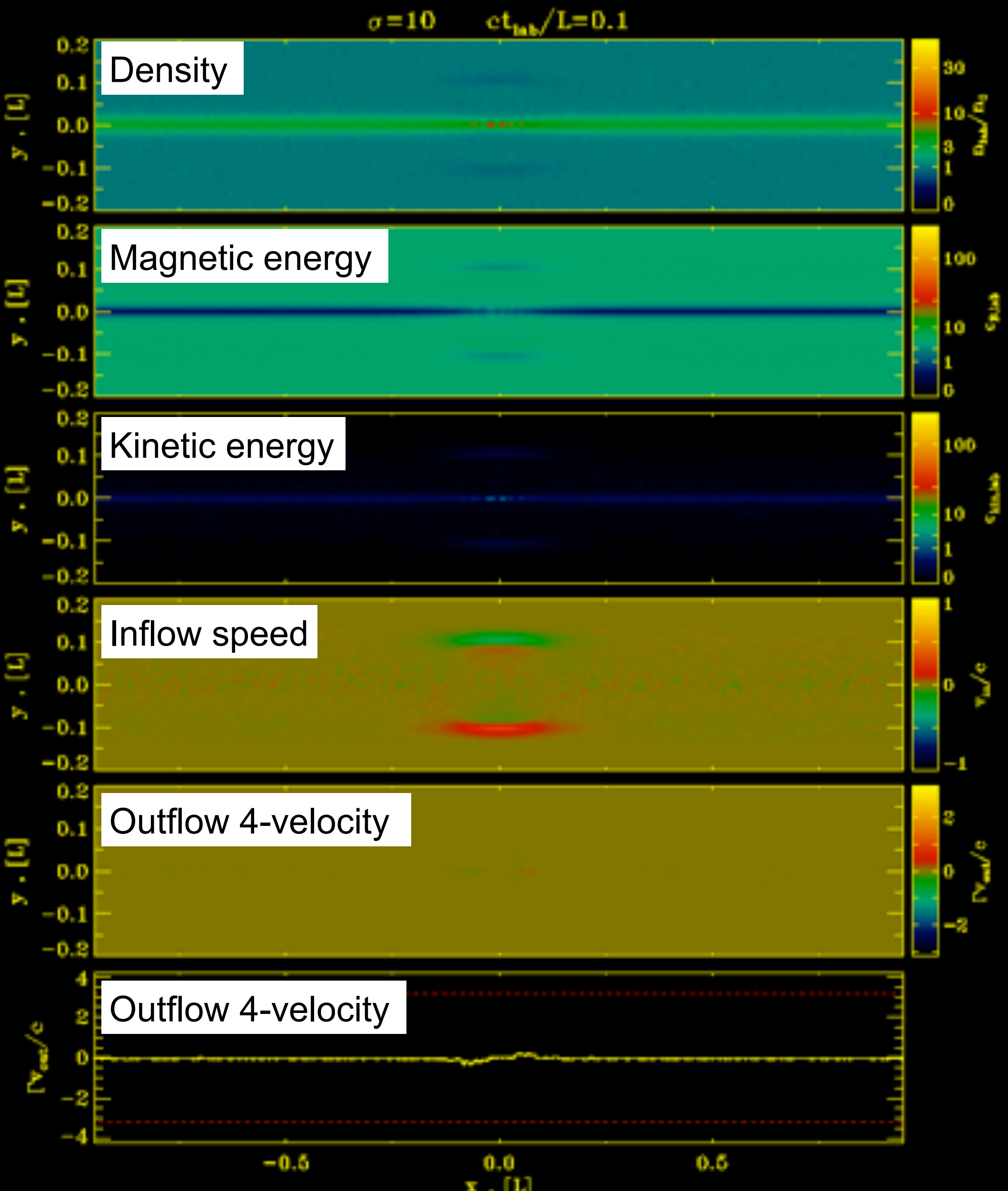

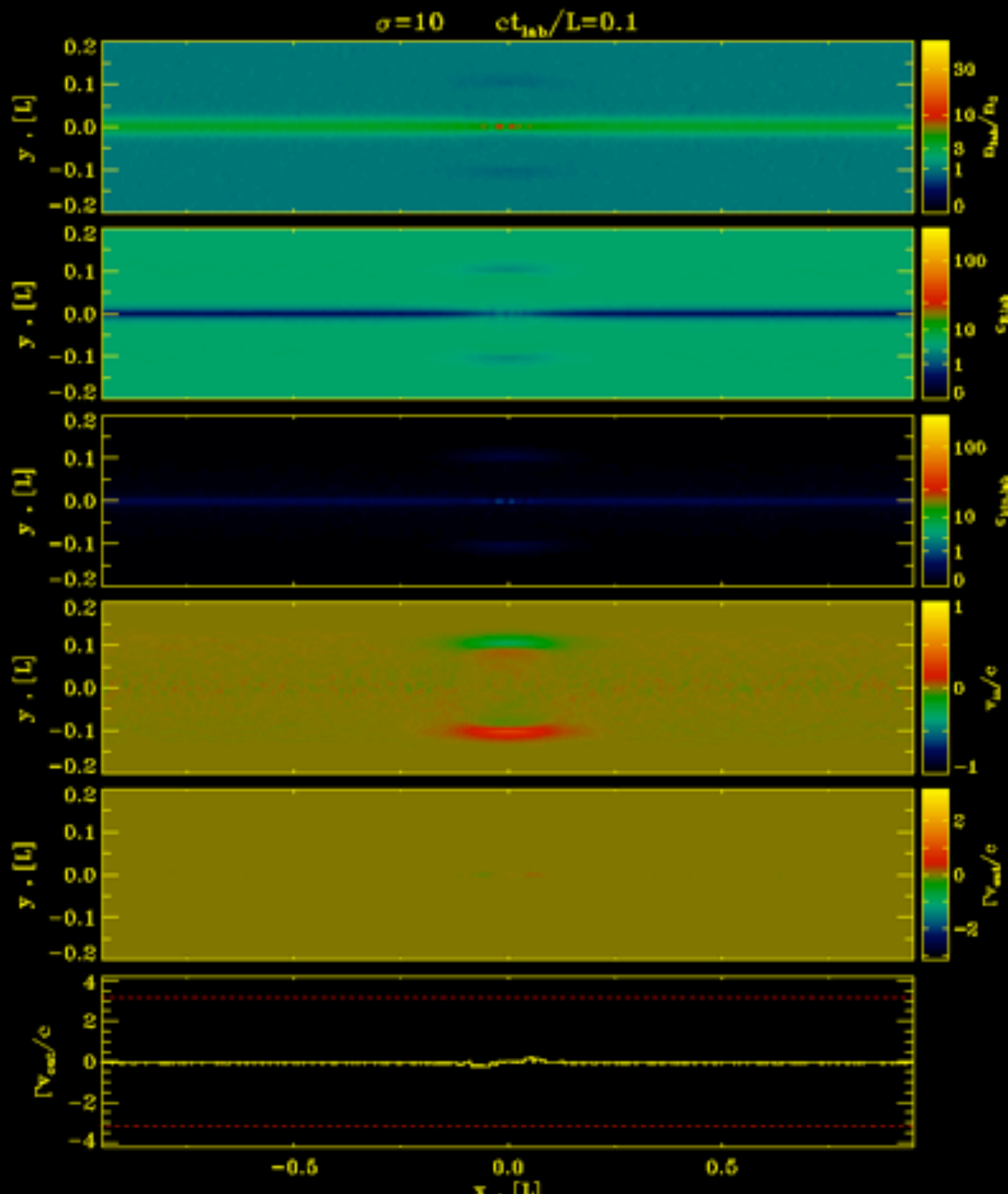

Strong IC losses

Inflow speed / c

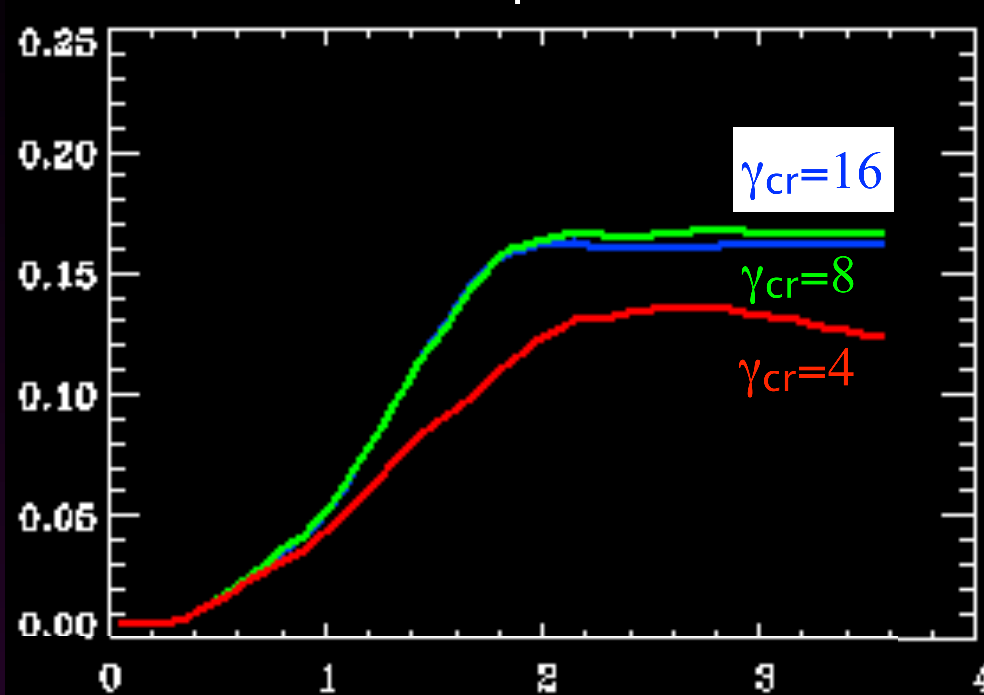

ct/L

Outflow 4-velocity / c

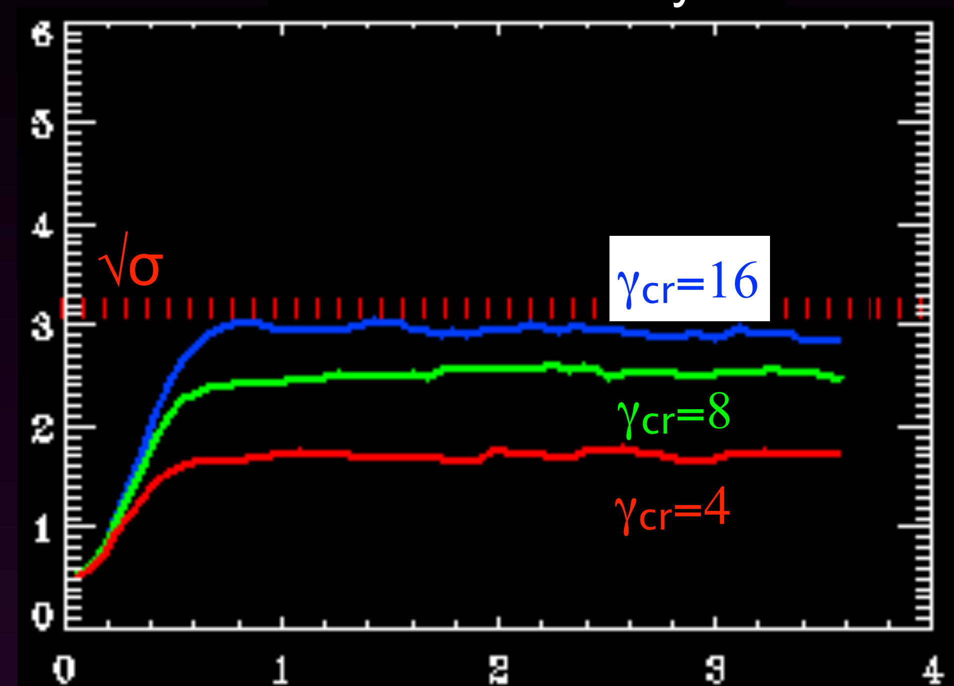

ct/L

No appreciable difference in the inflow speed (i.e., the reconnection rate).

Strong suppression in the maximum outflow 4-velocity (Compton drag).

4. Mimicking a large-scale compression (or expansion) in a PIC box

Velocity-space instabilities

- In accretion flows, as a result of shear or compression, the magnetic field is amplified.

- The particle magnetic moment is conserved.

$$\mu = \frac{mv_\perp^2}{2B}$$

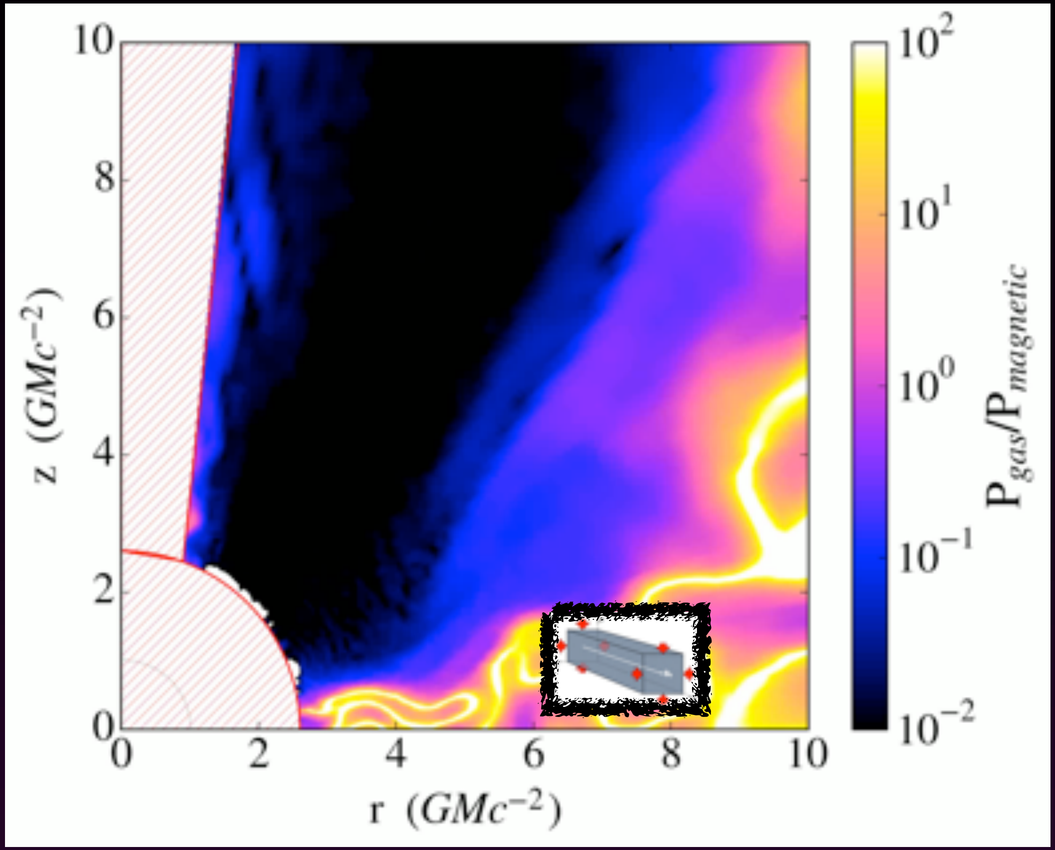

- This results in velocity-space anisotropies, with the particle pressure perpendicular to the field larger than along the field.

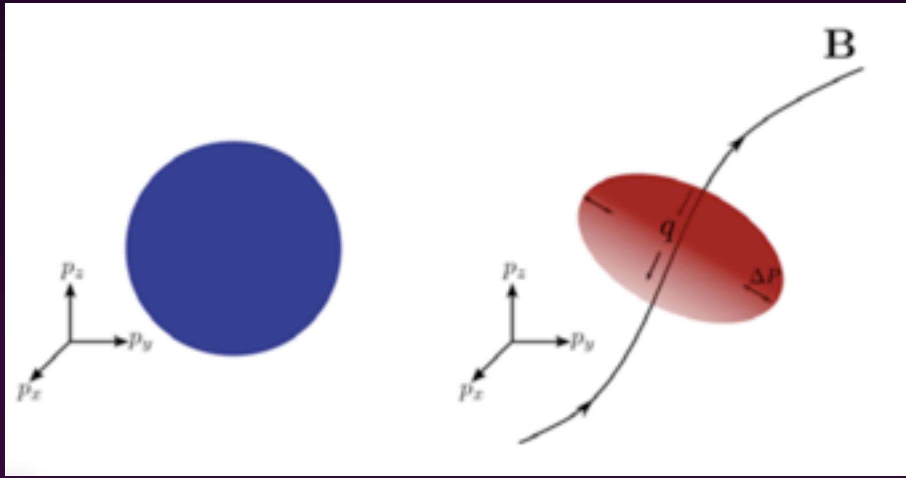

- How can this be accounted for, in a local PIC description?

Local PIC simulations of accretion flows

- We account self-consistently for a large-scale compression (or expansion), via a modified form of the PIC equations.

Unprimed coordinate system: with a basis of unit vectors, so it is the appropriate coordinate set to measure all physical quantities.

Primed coordinate system: with unit length of the spatial axes re-defined such that a particle subject only to compression/expansion stays at fixed coordinates.

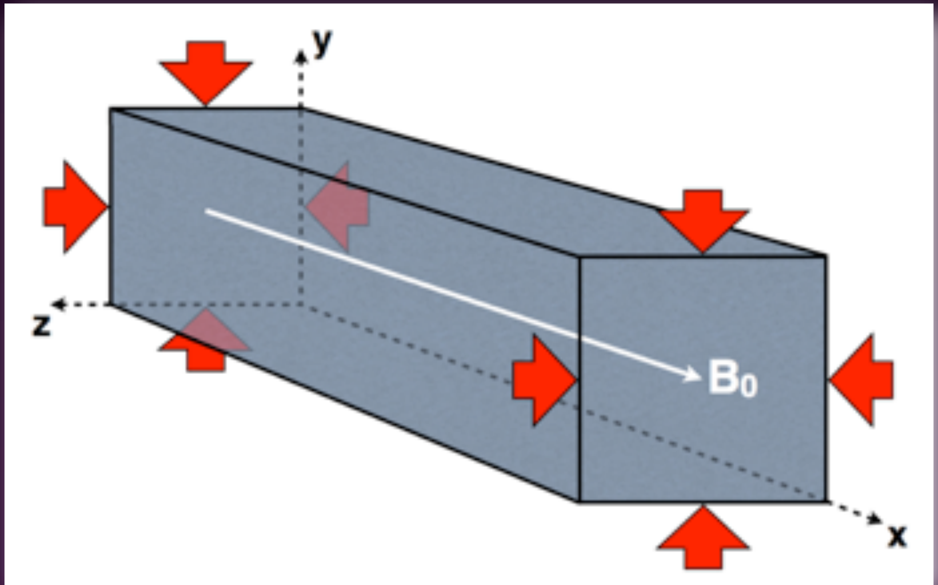

Compression Matrix

$$\boldsymbol{L} = \frac{\partial \boldsymbol{x}}{\partial \boldsymbol{x}'} = \begin{pmatrix} 1 & 0 & 0 \\ 0 & (1+q\,t)^{-1} & 0 \\ 0 & 0 & (1+q\,t)^{-1} \end{pmatrix}$$

$$\ell = \det(\boldsymbol{L}) = (1+q\,t)^{-2}$$

q = compression rate

Maxwell and Lorentz in a compressing box

In the limit $|\dot{\boldsymbol{L}}\,\boldsymbol{x}'|/c \ll 1$ of non-relativistic compression speeds ($\dot{\boldsymbol{L}} = \mathrm{d}\boldsymbol{L}/\mathrm{d}t$), and neglecting acceleration terms:

Maxwell's equations

$$\nabla' \times (\boldsymbol{L}\boldsymbol{E}) = -\frac{1}{c}\frac{\partial}{\partial t'}(\ell\,\boldsymbol{L}^{-1}\boldsymbol{B}) \quad ,$$

$$\nabla' \times (\boldsymbol{L}\boldsymbol{B}) = \frac{1}{c}\frac{\partial}{\partial t'}(\ell\,\boldsymbol{L}^{-1}\boldsymbol{E}) + \frac{4\pi}{c}\ell\,\boldsymbol{J}'$$

$$\boldsymbol{J}' = \boldsymbol{L}^{-1}\boldsymbol{J} = \ell^{-1}\sum_\alpha q_\alpha \boldsymbol{v}'_\alpha S[\boldsymbol{x}' - \boldsymbol{x}'_\alpha(t')]$$

$$\partial/\partial t' = \partial/\partial t$$
$$\nabla' = \boldsymbol{L}\,\nabla$$

→ CFL condition is more restrictive, and time-dependent

Lorentz force

$$\frac{\mathrm{d}\boldsymbol{p}}{\mathrm{d}t'} = -\,\dot{\boldsymbol{L}}\boldsymbol{L}^{-1}\boldsymbol{p} + q\left(\boldsymbol{E} + \frac{\boldsymbol{v}}{c} \times \boldsymbol{B}\right)$$

$$\frac{\mathrm{d}\boldsymbol{x}'}{\mathrm{d}t'} = \boldsymbol{v}' = \boldsymbol{L}^{-1}\boldsymbol{v}$$

→ automatically guarantees the conservation of the first and second adiabatic invariants

(Sironi & Narayan 15, Sironi 15)

Ion anisotropy-driven instabilities

- We account self-consistently for a large-scale field amplification.
- The resulting plasma anisotropy triggers the growth of instabilities.

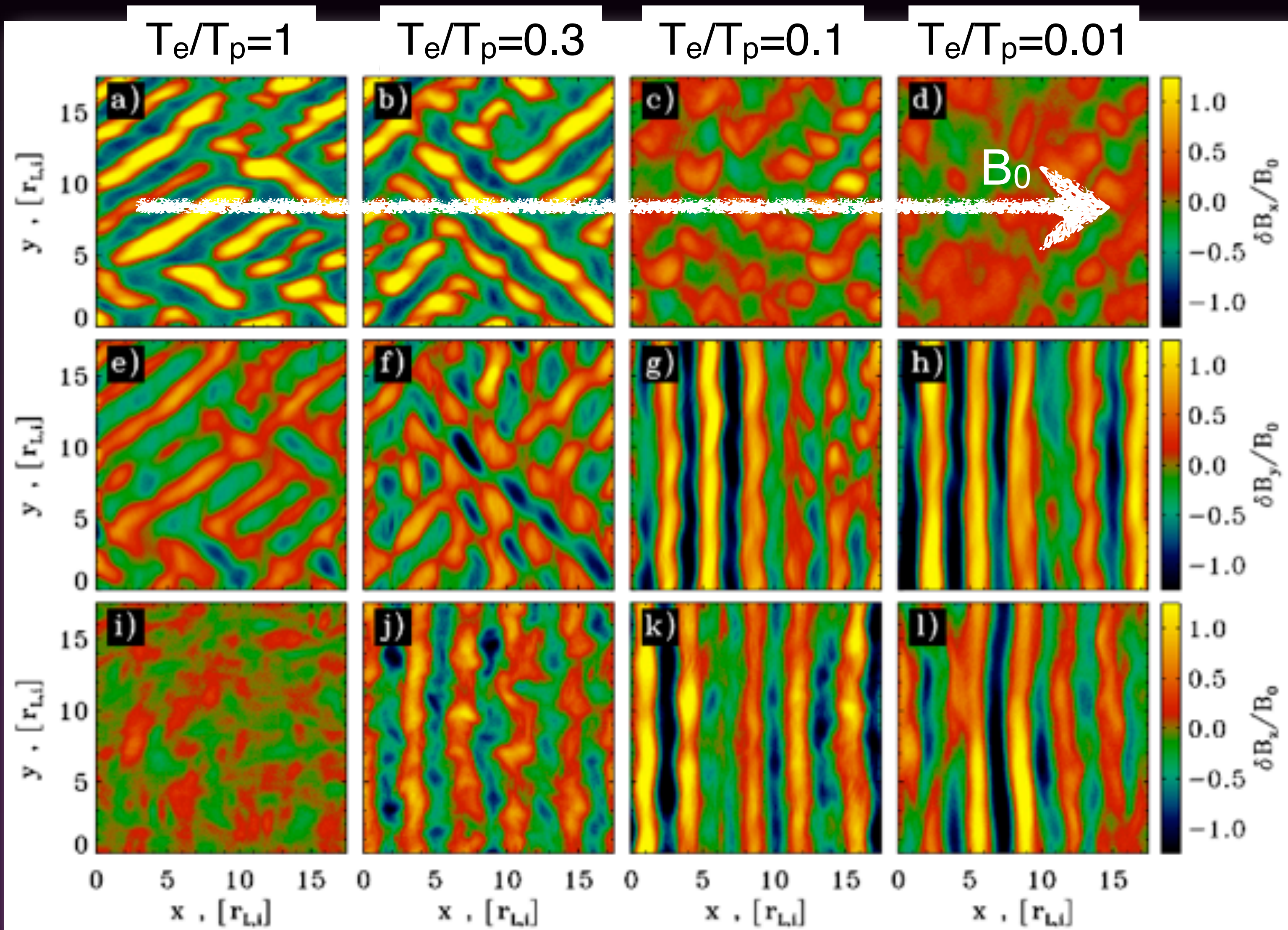

(Sironi & Narayan 15, Sironi 15)

- The nature of the dominant mode depends on the electron-to-proton temperature ratio.
- For low T_e/T_p<0.2, the ion cyclotron mode dominates (as opposed to the mirror instability).

Electron heating in accretion flows

We develop an analytical model to describe the efficiency of electron heating during the growth of the ion cyclotron instability.

(Sironi & Narayan 15, Sironi 15)

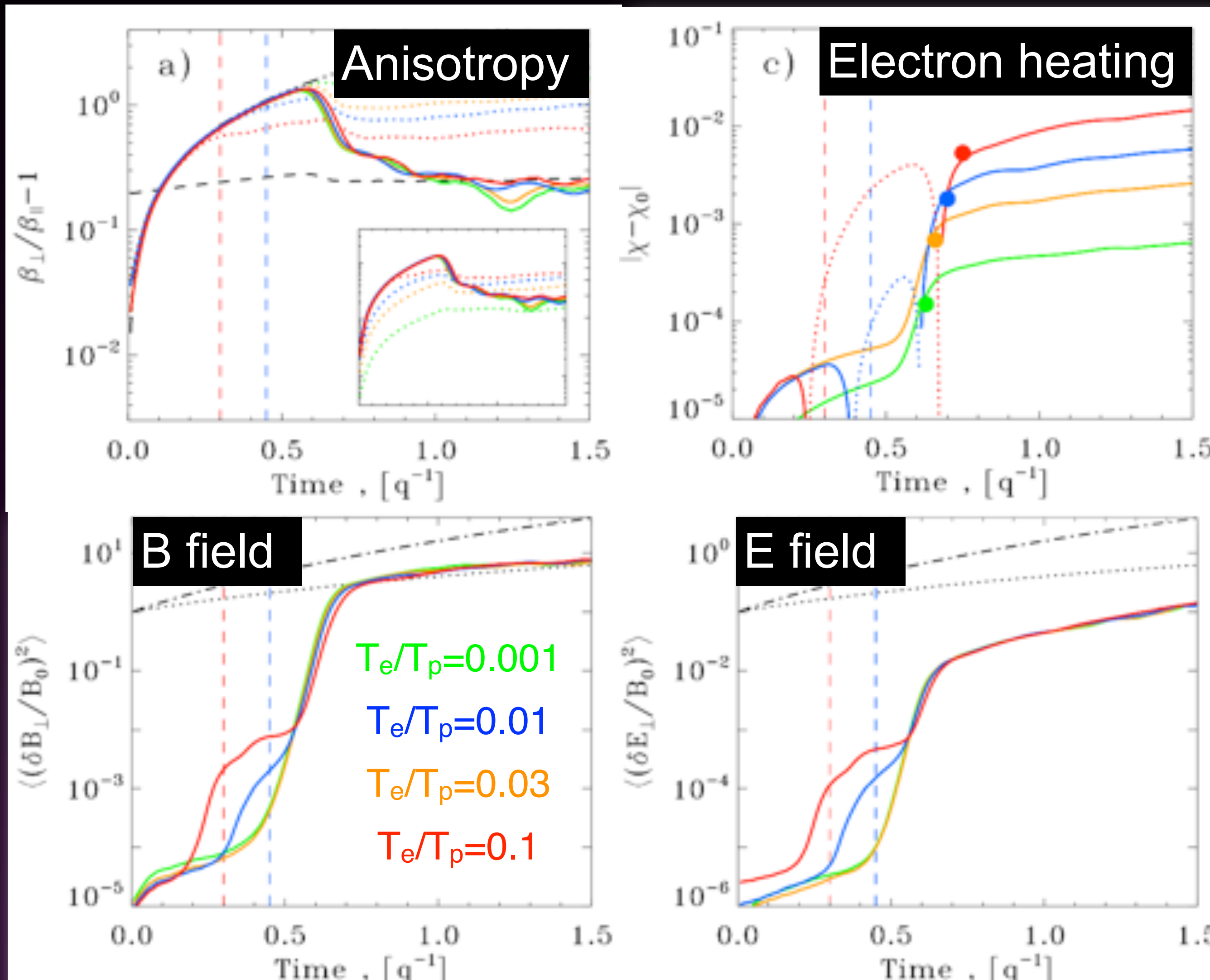

- We incorporate the PIC results as sub-grid physics in global general-relativistic magnetohydrodynamic simulations of collisionless accretion flows.

Summary

1. Ultra-relativistic magnetic reconnection ($\sigma \gtrsim 1$) in jets is an efficient particle accelerator, in 2D and 3D, with and without a guide field. The power-law slope is harder for higher magnetizations and weaker guide fields.

The largest plasmoids (with size ~0.1 L) contain the highest energy particles, with Larmor radius ~0.04 L, and are nearly isotropic (as assumed in MHD). Fast plasmoids can explain the extreme time variability of blazar flares.

2. In trans-relativistic reconnection ($\sigma \sim 1$), the power-law slope is harder for higher sigma and/or lower beta. Electron injection happens at X-points, which are more common for higher sigma and lower beta.

3. Compton drag in radiatively efficient accretion disk coronae can change the dynamics and statistics of reconnection plasmoids.

4. Large-scale MHD compressions or expansions can be accounted for in a local PIC description via a modified form of the PIC equations, that can be used to study electron heating in collisionless accretion flows or kinetic processes in jets/winds.